# Journal of Materials Chemistry A



## **REVIEW**

View Article Online
View Journal | View Issue



Cite this: *J. Mater. Chem. A*, 2017, 5, 13863

Received 5th March 2017 Accepted 17th May 2017

DOI: 10.1039/c7ta02007d

rsc li/materials-a

## Progress in catalytic synthesis of advanced carbon nanofibers

Wenyang Lu,<sup>a</sup> Ting He, <sup>Dd</sup> Bang Xu,<sup>a</sup> Xin He,<sup>a</sup> Hertanto Adidharma,<sup>a</sup> Maciej Radosz,<sup>a</sup> Khaled Gasem<sup>a</sup> and Maohong Fan <sup>D</sup>\*<sup>abc</sup>

Carbon nanofibers (CNFs) have wide applications in various high-tech areas. The demand for CNFs can exponentially increase due to the rapid development of advanced functional materials. Accordingly, a transformational progress is being made in synthesizing CNFs, especially functionalized CNFs. A dominant CNF synthesis pathway is catalytic chemical vapor deposition (CCVD). Therefore, the goal of this work is to review the most recent progress in CCVD synthesis of functional CNFs and to understand how the process conditions and catalysts, especially metal catalysts, affect the physical and chemical properties of the produced CNFs.

#### 1. Introduction

Carbon nanofibers (CNFs) are ultra-fine fibers with diameters below 800 nm that cannot be obtained using conventional approaches. In recent years, the production capacity for all carbon nanoproducts has increased dramatically, from 390 tons in 2008, ~500 tons in 2009, and ~710 tons in 2010, to over 9300 tons in 2015, representing a growth rate of 67% annually. Among these carbon nanomaterials, CNFs attracted great attention and research interest due to their promising performance and novel applications in electronic components and energy storage, and as polymer additives and catalyst support materials. 3-13

Geometrically, the morphology of CNFs is controlled by the nature of the catalysts used in synthesis and the interaction between the catalyst particles and carbon precursors.<sup>3,14-16</sup> In earlier studies, the differences between nanotubes and nanofibers were not strictly distinguished and both can be synthesized by using the vapor deposition method.<sup>17,18</sup> However, compared to nanotubes, nanofibers present a more delicate structure with more complexity in their spatial structure. As reported by Lakshmi *et al.*,<sup>18</sup> by increasing the deposition time, solid CNFs can be formed after the formation of carbon nanotubes (CNTs), while Hofmann *et al.*<sup>19</sup> reported that CNFs were typically synthesized at a relatively higher temperature compared to CNTs. Furthermore, from the perspective of the nanofiber/nanotube growth mechanism, Oberlin *et al.*<sup>20</sup> claimed that carbon diffuses over the surface of the metal

Unlike multi-walled CNTs that consist of seamless cylindrical graphene layers,22,23 CNFs consist of multiple layers of graphene with various stacking manners. As is known, graphene has excellent electronic, thermal, and mechanical properties that can significantly enhance the performance of the carbon materials. Nowadays, graphene can be synthesized using the chemical vapor deposition approach,<sup>24</sup> emulsion polymerization method<sup>25-27</sup> cationic surfactant-assisted chemical oxidative polymerization route,28 facile ultrasonic approach,29 in situ self-organization process30 and casting from the colloidal dispersion method.31 Moreover, attempts were made to improve the characteristics and properties of graphene. As reported by Son et al.,32 the compatibility of thermally reduced graphene was enhanced with increasing content of the PBT segment in the polyester. As shown in Fig. 1 Snoeck et al.33 reported that for units vapor-grown at high temperatures, catalyst particles can affect the diffusion path length and thus change the nucleation and excretion rates of carbon layers between the interfaces of solid-gas and solidliquid. At the same time, the formation of carbon layers, controlled by the adsorption and decomposition of carbon sources, is dominated by the interaction between catalyst particles and carbon precursors. Therefore, the diversity of the structure of CNFs provides the potential for obtaining the desired characteristics and properties of CNFs by modifying the parameters of synthesis. Therefore, the catalyst structure and reaction conditions tend to play a key role in designing CNF properties.

catalyst and forms a tubular structure from the circumference of the catalyst, and Rodriguez *et al.*<sup>21</sup> proposed that angled graphene layers are precipitated from a faceted catalyst particle to form a nanofiber. Since CNTs are not the key topic of this review, more attention will be focused on CNFs associated with their growth mechanism.

<sup>&</sup>lt;sup>a</sup>Department of Chemical & Petroleum Engineering, University of Wyoming, Laramie, WY, 82071, USA. E-mail: mfan@uwyo.edu

<sup>&</sup>lt;sup>b</sup>School of Energy Resources, University of Wyoming, Laramie, WY, 82071, USA

School of Civil & Environmental Engineering, Georgia Institute of Technology, Atlanta, GA, 30332, USA

dIdaho National Laboratory, Idaho Falls, ID, 83415, USA

Fig. 1 Structures of (a) a multi-walled CNT; (b) a graphene platelet; (c) a graphene fishbone; (d) a graphene ribbon and (e) a stacked-cup CNF<sup>23,34</sup> [reproduced with permission from ELSEVIER. Copyright ELSEVIER 2006].

Generally, CNFs are obtained from two major carbon resources: fossil hydrocarbons<sup>35</sup> and biomass.<sup>36,37</sup> The former has been investigated for a long time, while the latter is a more recent development still characterized by relatively low efficiency and high costs<sup>38–43</sup> Nonetheless, according to a recent research report,<sup>44</sup> the potential for using biomass feedstock in synthesizing CNFs is seriously underestimated. The major problem left in this area is that there is still no satisfactory synthesis route for producing high performance CNFs on a large scale and with a high yield.

Thus far, various technologies have been exploited for producing desired CNFs worldwide. 45-48 Arc discharge, 49 laser ablation,50 electrospinning,51,52 and catalytic chemical vapor deposition<sup>53</sup> (CCVD) are the major examples of synthesis approaches to making CNFs. Moreover, other methods were developed in order to improve the synthesis efficiency. Reddy et al.54 reported a simple one-step synthesis route for coating multi-walled CNTs on the basis of Fehling's reaction. As discussed in the book edited by Ebbesen,55 arc discharge and laser ablation cause the elimination of fixed carbons from the fibers, which results in their poor purity. By contrast, the CNFs fabricated from electrospinning and CCVD methods are of higher quality,56,57 but the ability of upscaling of CNFs produced from electrospinning is relatively weaker compared to those produced from CCVD,58 and the clogging of the Taylor cone59 and the low numbers of the Taylor cones<sup>60</sup> are the main problems that limit the yield of CNFs. In addition, the electrospinning parameters in electrospinning that control the properties of CNFs differ considerably from those of conventional chemical operations, including the electric charges of the jet, the stability of the jet path, the morphology of the jet and the angle of placing the Taylor cone, which increases the complexity of spinning thus restricting the capacity for the large-scale production of CNFs. 61-64 On the other hand, the yield of CNFs using the CCVD method is higher and the operation of CCVD is easier than that of the electrospinning method. 65 The existence of metallic catalyst particles contributed to the growth of fibers steadily and increased the CCVD selectivity process thus leading to a high possibility of producing CNFs on a large scale with relatively higher quality as reported by Liu et al.66 Therefore, from the application point of view, this review will focus on the catalytic vapor growth of nanofibers.

## 2. Catalytic chemical vapor growth of carbon nanofibers

#### 2.1 Chemical vapor deposition

The history of chemical vapor deposition (CVD) can be traced back to as early as the 19<sup>th</sup> century.<sup>67</sup> Initially, this method was intended to create diamond.<sup>68-70</sup> The first patent was issued in 1962 to Eversole<sup>71</sup> for synthesizing diamond using the CVD method. Unlike natural diamond formation, synthetic pure diamond was obtained by atomic hydrogen reacting with highly reactive hydrocarbon species.<sup>72</sup>

As for carbon nanofibers, the first patent was granted in 1889 for the synthesis of carbon nanofibers in carbon containing gases using metal catalysts,<sup>73</sup> which is an early version of vapor grown CNFs. Nowadays, CVD has evolved into the most popular method for synthesizing CNFs.<sup>74,75</sup> One of the advantages of CVD is a higher purity of carbon products compared to other methods.<sup>76,77</sup> Fig. 2 shows a conceptual drawing of a CVD process, where mixed-gas sources (*e.g.* CH<sub>4</sub> and H<sub>2</sub>) are

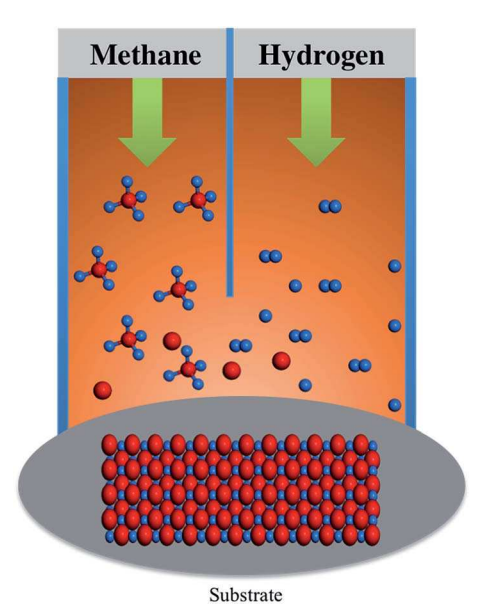
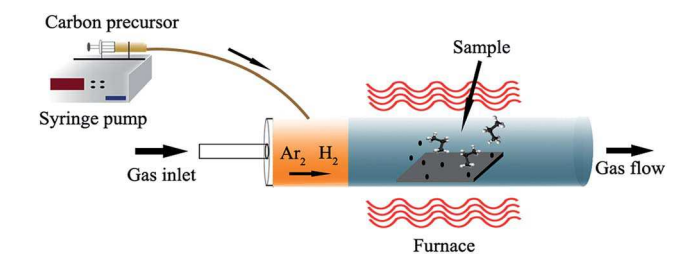


Fig. 2 Conceptual drawing of a CVD process using methane and hydrogen as gas sources.  $^{80}$ 



Schematic of a typical thermal CCVD process.

introduced into a vacuum chamber depositing a thin film of carbon materials on the substrate. Typically, a thin slice of a semiconductor (usually silicon crystal78,79) substrate is exposed to gas or liquid precursors, which react with catalysts on the surface of the substrate to produce the desired deposition.

Generally, a CVD process can be initiated or promoted by heat<sup>81-83</sup> (thermal CVD) and high frequency radiation (photo-CVD or plasma-CVD).84-87 Catalyst-assisted CVD is another specific type of CVD that utilizes metallic catalyst particles to react with carbon precursors. Fig. 3 is a schematic illustration of a CVD process for growing carbon materials, including carbon precursor (usually hydrocarbon) decomposition and carbon atom rearrangement into carbon species with the aid of metallic catalyst particles. In this process, the carbon precursor is pumped through a quartz tube that is located upstream of a horizontal tube furnace,88 and a substrate is located at the middle of the furnace in order to collect the nanofibers. The reaction between the carbon feedstock and catalyst particles occurs on the surface of the substrate in an environment of Ar and H2.

#### 2.2 Carbon precursors

As discussed in the previous section, the decomposition of carbon precursors and the diffusion of carbon atoms through metal-catalyst particles are key processes in CCVD. Originally, conventional fossil-based hydrocarbons, such as petroleum coke, coal pitch and charcoal,89-93 were the most commonly used raw materials, and the world benefited from these raw materials because of their relatively high yield, low cost, and abundant availability in nature. However, with decreasing supply of fossil fuels and increasing need for energy, renewable and natural substitutes are in short supply. As these substitutes are inexpensive, renewable, and abundant, great attention has been paid to this virgin territory, including the use of biomass as the carbon precursor in the synthesis of CNFs and other carbon materials. For example, lignocellulose, including lignin, bacterial cellulose, and resin, has been successfully converted into carbon precursors.94-98 As reported by Hiremath et al.99 a multi-step process for converting cellulose into carbon fibers was developed.

Generally, the selection of hydrocarbon sources in metal-free processes has a relatively minor effect on the growth of CNTs/ CNFs. 100 However, in the CCVD processes, the carbon source can be the vital factor that may affect the structure of the CNFs/

CNTs. As reported by Muradov et al., 101 thermal decomposition of methane as the precursor leads to amorphous carbon rather than CNFs or CNTs at 800-900 °C. Zeng et al.100 reported that bamboo-like CNTs were obtained through ethylene decomposition and turbostratic CNFs were produced with the use of acetylene as the precursor. Titirici et al. 102 pointed out that biomass hydrothermally transformed into carbonaceous structures is chemically and spectroscopically similar to peat or lignite, depending on the time and temperature. The additional components existing in the plant material can contribute to the formation of nanostructures. As reported by Hu et al., 103 CNFs/ CNTs synthesized from biomass at high temperature displayed a higher carbon content compared to CNFs/CNTs obtained at low temperature. Moreover, metal ions can speed up the reaction and produce hierarchical structures of CNFs and CNTs.

Cagnon et al. 104 reported that the composition of biomass in lignocellulose has a strong relationship with the nanostructure of generated products. Kadla et al. 105 indicated that increasing the carbon content in the precursor would increase the lengths of fibers generated. The ratios of carbon to hydrogen for hemicellulose, cellulose, and lignin are 6.4, 6.5 and 10.3, respectively. Fig. 4 shows the weight fractions of the biomass composition in lignocellulose. From the data provided in Fig. 4 and the ratio of carbon to hydrogen obtained from the experiment conducted, it is clear that lignin and cellulose contributed the most to the formation of CNFs. Lately, Koziol et al. 106 proposed a method to chemically modify lignin in order to improve its fiber spinning performance using polyethylene oxide, and the results indicated that the spinning temperature for a single fiber could be reduced by up to 45 °C. Other studies included carbonization, 107,108 char activation 109,110 (char is generated from the conversion of biomass), and precursor preparation.111,112 These studies demonstrate that no matter which kind of raw material is selected, it will eventually convert into a gaseous carbon-containing precursor for CCVD, despite some differences in dealing with different kinds of raw materials. These studies also tell us that it is the catalytic reactions during the fiber growth that determine the properties of the fibers produced, rather than the precursor preparation methods.

Next, we shall discuss the factors that affect the formation of CNFs, mechanisms of catalysts reacting with carbon precursors, and characteristics of catalysts applied.

#### 3. Catalysts used in catalytic chemical vapor deposition of carbon nanofibers

#### 3.1 Mechanisms of catalytic chemical vapor deposition

Metal catalyst particles play a significant role in catalyzing the growth of CNFs. Transition metals such as iron, cobalt and nickel are the most commonly used catalysts in synthesizing CNFs, though vanadium, molybdenum, chromium and ruthenium have also been studied.33,123-127 There is some controversy about the mechanisms of the catalytic growth of CNFs. Initial studies128 indicated that the formation of CNFs starts from the detachment of catalyst particles, after which carbon precursors

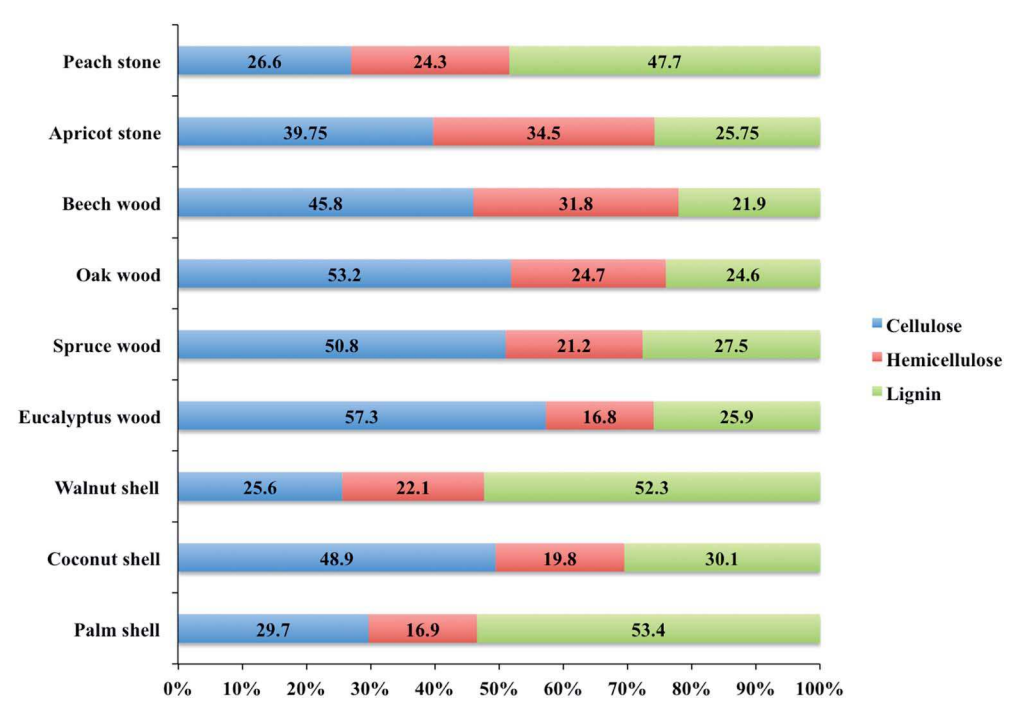


Fig. 4 Weight fractions of lignocellulose composition biomass<sup>113-122</sup> [reproduced with permission from ELSEVIER. Copyright ELSEVIER 2010].

decompose and distribute on the surface of the detached catalyst particles where the growth occurs. By contrast, Kock *et al.*<sup>129</sup> claimed that in the progress of CCVD, unstable carbide is formed that causes the reconstruction of the catalyst particles, and then the carbide decomposes into very few nanofibers and metal particles. However, Alstrup *et al.*<sup>130</sup> reported that no major reconstruction could be observed in an experiment using Ni–Cu alloy catalysts for synthesizing CNFs, which suggests that bulk carbide formation is not likely. The efforts to determine the formation mechanism of CNFs lasted for years, <sup>131–133</sup> and are likely to continue.

The chemical states of the metal catalyst particles and their movement paths have also been studied extensively. Yu *et al.* <sup>88</sup> reported that the chemical states of nickel catalysts influence the growth of CNFs. The chemical states of catalysts may greatly affect the structure and characteristics of the products too. <sup>134,135</sup> Typically, the chemical states of nickel catalysts include metallic nickel (Ni), nickel sub-carbide (Ni<sub>3</sub>C<sub>1-X</sub>), nickel carbide (Ni<sub>3</sub>C), NiO, Ni(OH)<sub>2</sub> and NiOOH. <sup>136</sup> Bowen's group investigated Ni, Ni<sub>3</sub>C<sub>1-X</sub> and Ni<sub>3</sub>C during CNF growth, including Ni<sub>3</sub>C at 300 °C, composite Ni–Ni<sub>3</sub>C<sub>1-X</sub> between 400 and 500 °C and metallic Ni at 600 °C. The results show that with increasing temperature, the Ni catalyst changes its chemical state from a single element to a metal containing carbide. Subsequently, the metal containing carbide eventually controls the structure of the produced CNFs.

In order to calculate a metal's capability of forming and breaking bonds at its surface, the thermodynamics of the carbonization equation<sup>137</sup> is used:

$$M_z + C_x H_y \to M_z C_x + \frac{1}{2} y H_2$$
 (1)

where M denotes a metal,  $C_xH_y$  a carbon source and  $M_zC_x$  the corresponding metal carbide. The Gibbs free energy of the reaction can be written as

$$\Delta G = \Delta H - T_{\rm r} \Delta S \tag{2}$$

$$\Delta H = \Delta_{\rm f} H_{\rm M_2C_x}^{\circ} - \Delta_{\rm f} H_{\rm C_xH_y}^{\circ} \tag{3}$$

where  $\Delta H$  is the enthalpy,  $T_{\rm r}$  is the temperature,  $\Delta S$  is the entropy,  $\Delta_{\rm f} H_{\rm M_2 C_x}^{\circ}$  is the standard enthalpy of formation of the metal carbide, and  $\Delta_{\rm f} H_{\rm C_x H_y}^{\circ}$  is the standard enthalpy of formation of the carbon source. Generally, the complex metal types containing carbides can vary widely along with the operating conditions. The mechanisms of carbon atoms reacting with the metal particles and the carbide decomposition are poorly understood. Blank *et al.*<sup>138</sup> reported that Fe-carbides that contain a high amount of carbon were observed below 1000 °C in the growth of fibers using TEM. Hagg carbides (x-Fe<sub>5</sub>C<sub>2</sub>) and cementite ( $\theta$ -Fe<sub>3</sub>C) have been obtained. Only x-Fe<sub>5</sub>C<sub>2</sub> was observed to decay into cementite and y-Fe, while the other Fecarbides ( $\theta$ -Fe<sub>3</sub>C) were not affected at all.

$$Fe_5C_2 \rightarrow Fe_3C + \gamma - Fe$$
 (4)

The movement of catalyst particles starts from the sharp edges of the metal, and then the particles begin to split into two parts (Fe-carbides). With the increase of irradiation, the two fragments of catalyst particles start to move along the fiber in the opposite direction. At the end of this motion, the particles stop changing their fiber shape, volume, and location. These processes are shown in Fig. 5.

The catalyst efficiency is measured by its ability to decompose the hydrocarbon precursors and to contribute to carbon

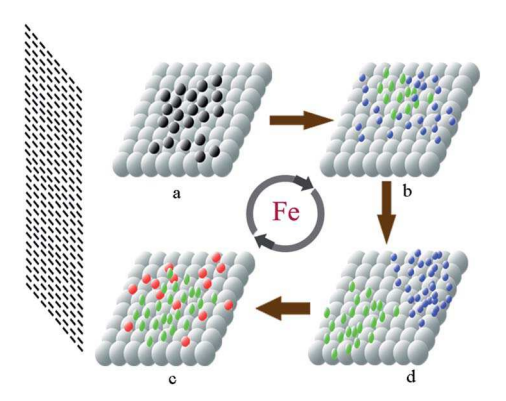


Fig. 5 (a) CNF containing catalyst particles in the middle; (b) catalyst particles split into two Fe-carbides (Fe<sub>5</sub>C<sub>2</sub> and Fe<sub>3</sub>C); (c) the two Fecarbides move along the opposite direction of the nanofibers; (d) Fe<sub>5</sub>C<sub>2</sub> splits into Fe<sub>3</sub>C and  $\gamma$ -Fe.

diffusion. Abild et al. 139 performed Density Functional Theory (DFT) modeling and found that there exists a preference for carbon precursor decomposition and adsorption at different sites of the catalyst (nickel (111) and (211)), as shown in Fig. 6. Compared to structures (a) and (d), structures (b) and (c) have the lowest adsorption energies, -0.45 eV and 0 eV, respectively, which means that with increasing adsorption energy, the nucleation of graphene preferentially occurs at the step edge sites.

Other particle sites investigated by Hofmann et al. 140 showed that the energy barrier of C diffusion on the Ni (100) site is around 1.9 eV, which is much higher than those on the Ni (111) and Ni (211) sites. An energy barrier of 0.5 eV for the free Co (111) surface and a similar barrier for Ni (110) (0.4 eV) was calculated

by DFT modeling. Saadi et al.141 reported the adsorption energies of a carbon atom at different metal sites, which are shown in Table 1. The adsorption energies of catalysts Ni, Ru, Rh and Co are the lowest at half coverage, which means that the carbon atoms stick together tighter on the step-edge sites than on the terrace. Only Ni, Fe and Co managed to form stable graphene layers showing that there exists an energetic driving force for the formation of graphene layers, 142 which demonstrated that the carbon atoms tend to decompose and diffuse on the step-edge sites of the metal particles. Moreover, the Co catalyst displayed even lowered carbon adsorption energy upon incorporation of carbon into a finite-graphene layer adsorbed at the step edge, which matches the adsorption energy for Ni indicating that the step edges on both metal surfaces may act as the preferential nucleation sites for graphene. Since the graphene layers formed by strained Ni, Ru and Rh are not stable because the formation of a nucleus of this finite size is energetically unfavorable, the growth of graphene is hindered on these surfaces. The instability indicates that 3d group metals such as Co and Ni are more favorable for the formation of graphene layers. It should be noted that the graphene layers formed by Fe are not stable throughout this process. Even though Fe is one of the 3d group metals, in contrast to hcp and fcc metals, Fe displays closepacked surface sites. Based on DFT calculations, C is more stable at the 5-fold coordinated step site on the Fe (310) surface than at the 4-fold coordinated step sites on the Fe(321) surface. In the middle of the process of formation of graphene layers, a carbide was formed temporarily, and then the metalcontaining carbide decomposed and let the carbon atoms diffuse onto different sites of the metal particles. Thus, the Fe step site cannot be considered as an ideal nucleating center for the formation of graphene.

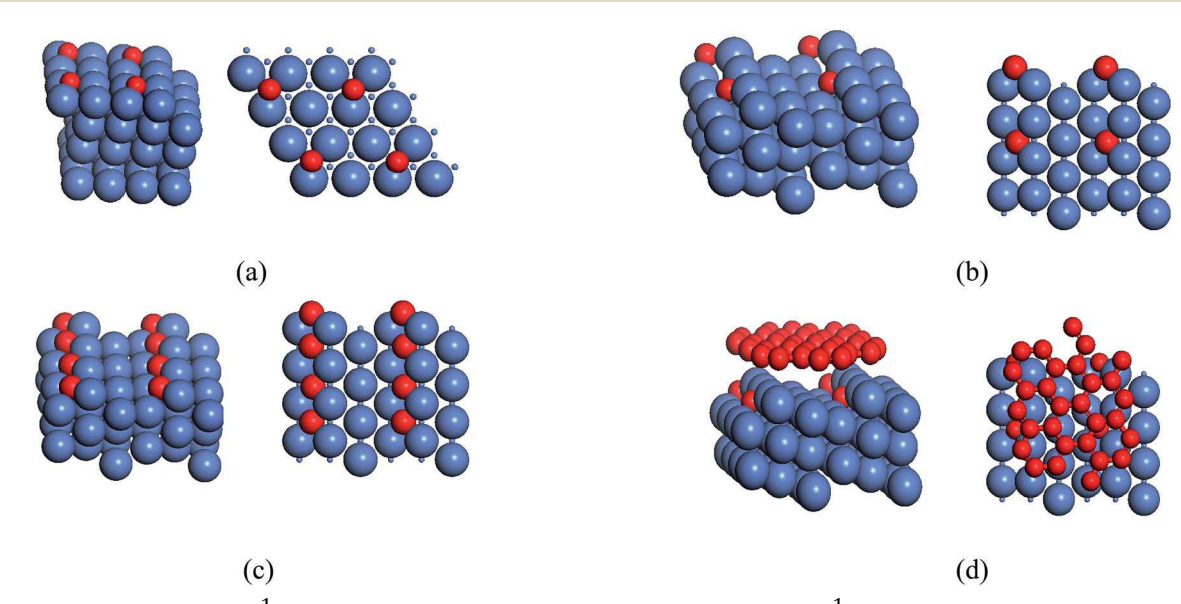


Fig. 6 (a) Ni (111) hcp site with  $\theta_{\rm C} = \frac{1}{4}$  ML and  $E_{\rm ads} = 0.55$  eV; (b) Ni (211) step-edge site with  $\theta_{\rm C}^{\rm st} = \frac{1}{2}$  and  $E_{\rm ads} = -0.45$  eV; (c) Ni (211) step-edge site with  $\theta_{\rm C}^{\rm st} = 1$  and  $E_{\rm ads} = 0$ ; (d) interface hcp site on Ni (111) with  $\theta_{\rm C} = \frac{1}{4}$  ML and  $E_{\rm ads} = 0.92$  eV. <sup>139</sup> \*The coverage  $\theta_{\rm C}^{\rm st}$  is the  $N/N_{\rm tot}$  ratio, where N is the number of carbon atoms adsorbed and  $N_{\text{tot}}$  is the total number of step-edge atoms.  $\theta_{\mathbb{C}}$  is the surface coverage in the monolayer [reproduced with permission from American Physical Society. Copyright American Physical Society 2006].

Table 1 Adsorption energies of a carbon atom at different metal sites 141a

Surface	Ni (eV)	Ru (eV)	Rh (eV)	Ni <sub>strained(9%)</sub> (eV)	Fe (eV)	Co (eV)
Terrace	1.25	0.80	0.64	1.00	0.40	1.20
$ heta_{ m C}^{ m st}=1/2$	0.25	0.10	0.28	0.26	(310) - 0.23 $(321) 0.50$	0.42
$ heta_{ ext{C}}^{ ext{st}}=1$	0.70	0.38	0.28	0.28	(310) -0.02 $(321) 0.95$	0.71
Graphene	0.15	Unstable	Unstable	Unstable	0.41	0.33

<sup>&</sup>lt;sup>a</sup> The coverage  $\theta_{\text{c}}^{\text{St}}$  is the  $N/N_{\text{tot}}$  ratio, where N is the number of carbon atoms adsorbed and  $N_{\text{tot}}$  is the total number of step-edge atoms.

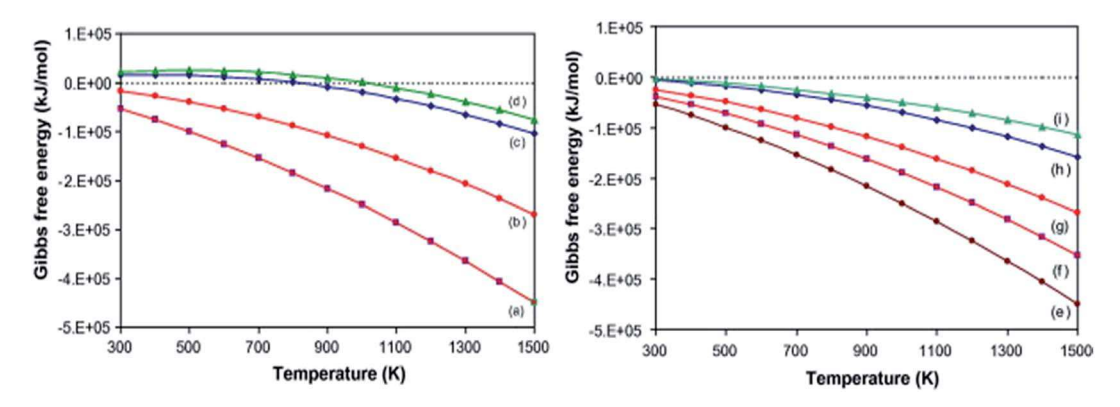


Fig. 7 Calculated changes in the Gibbs free energy for the reaction of Ni with (a) C<sub>2</sub>H<sub>2</sub>, (b) C<sub>2</sub>H<sub>4</sub>, (c) CH<sub>4</sub>, and (d) CO; for comparison, the calculated changes in the Gibbs free energy for the reaction of  $C_2H_2$  with (e) Ni, (f) Co, (g) Fe, (h) W, and (i) Mo are also provided <sup>143</sup> [reproduced with permission from ELSEVIER. Copyright ELSEVIER 2009].

Esconjauregui et al.143 calculated the Gibbs free energy for the reaction of nickel with different carbon sources and the Gibbs free energy of a single carbon source with different metal catalysts and the results are presented in Fig. 7. The nickel catalyst had the highest change of the Gibbs energy. This is because the ability of a transition metal to react with carbon increases with its number of electron vacancies in the d orbital, and frictional force can increase the number of d vacancies.144 Typically, the frictional force is the source of heat that increases the temperature. Ni is expected to form at a wide range of temperatures in the reaction with carbon sources. 137 At the same time, since the carbides formed with Fe are unstable, at the end of the reaction, these carbides will decompose and form nanomaterials.

Meanwhile, one of the challenges facing the formation of CNFs is the unsteady-state nature of diffusion and formation processes.145 Since the diffusion of carbon molecules and formation of CNFs are rate-determining processes, when the diffusion rate is lower than the formation rate, the catalyst is not fully utilized. Conversely, the excess carbon molecules clogging the surface of metal particles prevent the other carbon molecules from reacting with the catalyst, which lowers the yield of CNFs. Another challenge is that the graphite nucleation is inhibited by the extremely small size of catalyst particles. <sup>146</sup> For example, Park et al.147 claimed that the diameter of nickel particles could be as small as 1.5 nm. Such small particle sizes of catalysts can destroy the basic unit during the graphite

nucleation process. To determine the efficiency of catalysts utilized in synthesizing CNFs, multiple factors should be taken into consideration. How to relate the catalyst properties to the properties of the produced CNFs has been a subject of extensive research.139,148,149

#### 3.2 Factors affecting the performance of catalysts

#### 3.2.1 Composition effect

3.2.1.1 Limitations of single-metal catalysts. Both singlemetal catalysts and multi-metal catalysts have been used in the CCVD of CNFs. Catalyst particles can greatly improve the efficiency of carbon yields, and thus increase the yield of the produced nanofibers. 150,151 Ermakova et al. 152 reported that the yield of carbon reached as high as 384 g per 1 g of nickel catalyst. They also found that the carbon yield increased with increasing concentration of Ni in the catalyst, while the carbon precursor decomposition reached a maximum of 96%. Lately, Takenaka et al.145 demonstrated that Ni was the most effective catalyst among other metal catalysts (Mg, Al, Si, Ti, and Zr) and the CNF yield was 491 g per 1 g of Ni. Table 2 lists the structures of carbon species produced by different catalysts. Martin-Gullon et al. 153 reported iron-derived CNFs obtained at 1350 K, which is slightly higher than the spreading temperature in Table 2. Soot-like nanoballs and non-uniformity of the amorphous carbon were observed on the surface of the fibers. This observation was attributed to the fact that metal particles

Table 2 Correlation between the wetting properties of metal catalyst particles on graphite and crystallinity of CNFs produced<sup>137,153,155–160</sup>

Metal catalyst	Spreading temperature $^a$ (°C)	Type of carbon species	Diameter (nm)
Iron	1000	Amorphous	~25
Nickel	975	Amorphous	$\sim \! 25  140$
Cobalt	400	Highly graphitic	30-200
Platinum	755	Partially graphitic	$\sim \! 80$
Copper-nickel (3:7)	675	Moderately graphitic	$\sim \! 100  200$
Nickel-iron (1:1)	530	Highly graphitic	$\sim \! 20$
Ruthenium	535	Highly graphitic	~7
Iridium	965	Amorphous	${\sim}40$
Platinum-iridium (1:1)	850	Amorphous	_

<sup>&</sup>lt;sup>a</sup> Spreading temperature is defined as the point where metal particles undergo transition from wetting to spreading.

seeded over already formed fibers. These irregular metallic particles and amorphous carbon cause the growth of new fibers with smaller sizes and encapsulate the existing CNFs. This process can repeat several times in the reaction and lead to the amorphous nature of carbon species or graphene layers. Moreover, Rodriguez et al.154 reported that Cu-Ni presented a high activity toward the synthesis of CNFs at around 750 °C, while with the increase of temperature, the activity decreased significantly and when the temperature was lowered to 750 °C, the alloy catalyst reacquired its activity. It should be noted that by mixing Ni and iron, the spreading temperature dropped sharply, and the quality of the produced carbon species changed from an irregular morphology to highly graphitic, which means that the structure and properties can be improved by adjusting the ratio of the alloy constituent. Among these metal catalysts, pure cobalt forms highly graphitic CNFs at the lowest spreading temperature. Meanwhile, iron, nickel, and other catalysts show weaker interactions with graphite, and thus produce CNFs that contain a large fraction of amorphous carbon. Besides, when mixed with nickel, copper or iron catalyst particles, highly ordered CNFs tend to be generated. Therefore, the spreading temperature can not only indicate the chemical state change of the metallic catalyst, but can also predict the highest activity of the catalyst in the reaction. As such, it is possible to lower the operation temperature and thus lower the energy consumption and improve the degree of carbon nanostructure.

Initially, single metal catalysts were applied in the CCVD synthesis of CNFs. Singh et al.161 reported a novel method to synthesize herringbone-stacked CNFs using cobaltocene as a catalyst precursor below 110 °C. According to their initial tests, they concluded that using cobaltocene as the catalyst precursor at 140 °C gives the best performance and herringbone CNFs can be obtained with diameters of about 15 nm. They believed that the feedstock first reached the metal surface forming atomic carbon species, then dissolved into catalyst particles, and eventually precipitated forming graphite layers whose arrangement mainly depends on the location of catalyst particles.

However, single metal catalysts have their limitations. With relatively poor controllability in fiber growth, the length, diameter, and shape of carbon products cannot be manually controlled. This challenge not only affects the growth of carbon fibers, but also remains in the early stage of carbon nanotube synthesis. Ding et al. 162 did DFT calculation of the adhesion between single-walled CNTs (SWCNTs) and catalyst particles, and concluded that

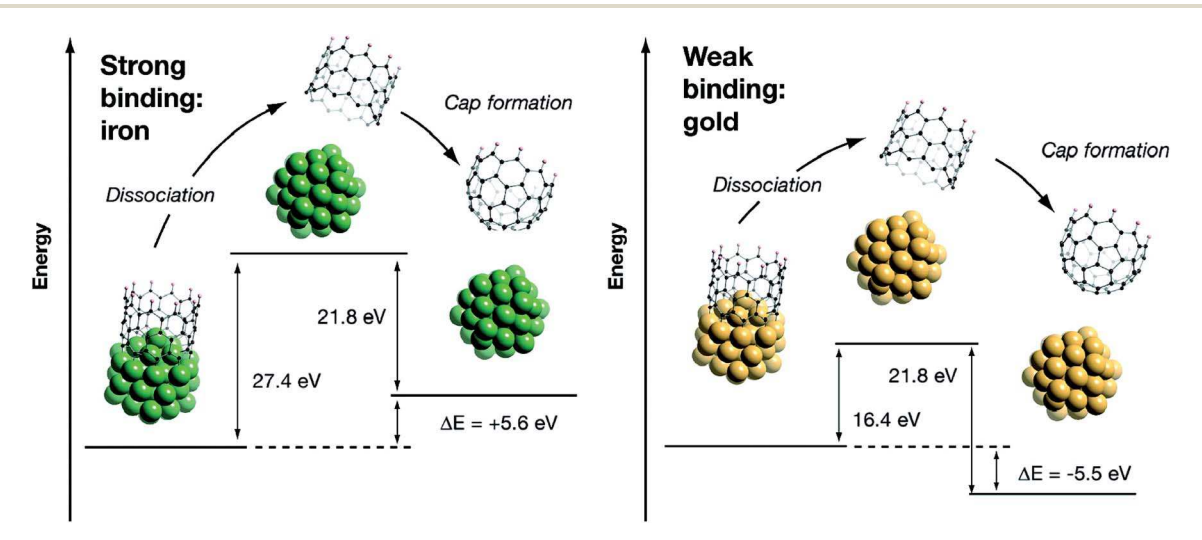


Fig. 8 Schematic illustration of the dissociation of a SWCNT from a metal catalyst particle<sup>162</sup> [reproduced with permission from American Chemical Society. Copyright American Chemical Society 2008].

Table 3 Solid carbon yield as a function of reactant composition over Fe-Cu (7:3) when reacted for 3 h at 600 °C (ref. 169)

Reactant gas ratio CO/C <sub>2</sub> H <sub>4</sub> /H <sub>2</sub>	Solid carbon yield (g of C per g of cat)		Structure
4:0:1	16.2	56	Spirals and coils
1:0:4	3.9	_	Spirals and coils
3:1:1	39.2	77	Platelet
1:1:3	30.9	109	Herringbone
1:3:1	78.3	81	_
0:1:4	25.6	_	_
0:4:1	1.6	23	_

nanotube growth needs strong adhesion, for example, as shown in Fig. 8. In order to maintain the constant and stable growth of CNTs in this reaction, the free energy  $(\Delta E)$  must be positive. Otherwise, a cap can be formed spontaneously and stop the growth of CNTs. At the end of the reaction, the metal with a high binding strength will prevent the spontaneous cap formation ( $\Delta E$ < 0), whereas the metal with a low binding strength will fail to prevent the cap formation ( $\Delta E < 0$ ).

This example clearly shows that some metals can improve the efficiency of CNF formation, but may fail to dissociate from the formed CNFs at the end of the reaction. To overcome this problem, multi-metal catalyst systems were explored toward increasing the binding strength between alloy particles and carbon atoms, and thus promoting the controllability of the produced CNFs.

3.2.1.2 Advantages of multi-metal catalysts. In order to manually control the properties of the produced CNFs, and to improve their yields, bi-metal and multi-metal catalysts have been investigated to synthesize carbon nanomaterials. 163-168 Iron-group elements (Fe, Co and Ni) and their corresponding alloys are the most common examples. However, extending the range of metals and their combinations is another approach to develop enhanced catalysts.

Carneiro et al. 169 reported a low-temperature (500-650 °C) CNF synthesis method using Fe-Cu catalysts. Their optimal reactant gas ratios are given in Table 3. They demonstrated that when the ratio of CO/C<sub>2</sub>H<sub>4</sub>/H<sub>2</sub> was 1:3:1, maximum solid carbon yields were obtained. At 600 °C, the fiber grew as a "platelet" structure. 170,171 When the ratio of Fe-Cu reached 9:1, the structure changed from platelet to tubular, and when the ratio became 7:3, the structure changed to fishbone. It is believed that CO activates the metal particles, which in turn causes the decomposition of  $C_2H_4$  by inducing surface reconstruction, <sup>172</sup> and the  $\pi$  of CO becomes the electron acceptor resulting in electronic perturbations that break the C=C bond.169

Bimetallic catalyst systems show the potential to control the structure of CNFs. This is because the second metal in bimetallic catalysts enhances the geometric and electronic effects

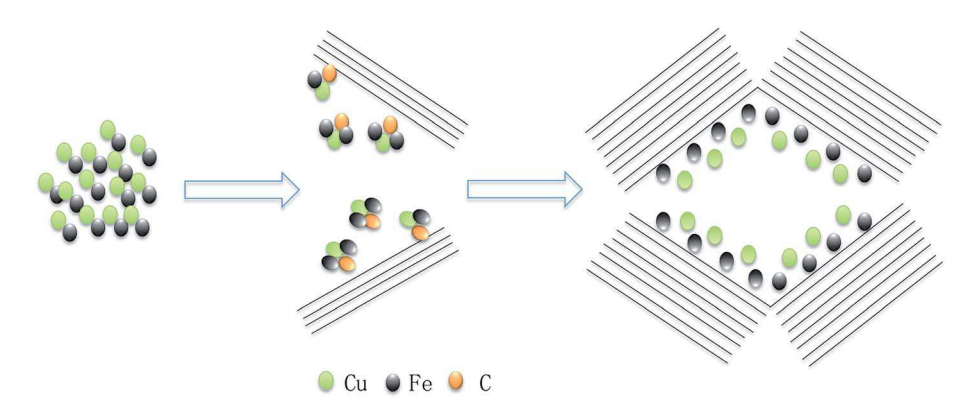


Fig. 9 Interaction between Fe/Cu catalysts and the solid carbon interface.

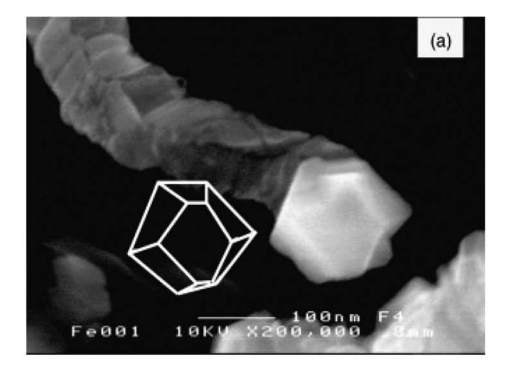




Fig. 10 Highly magnified HR-SEM images of Fe catalysts on the top of (a) platelet and (b) tubular CNFs<sup>174</sup> [reproduced with permission from ELSEVIER. Copyright ELSEVIER 2004].

Table 4 Comparison of the physical and structural characteristics of "platelet" carbon nanofibers produced from different catalytic reactions 176

Catalyst	Feedstock	Space velocity (mL h <sup>-1</sup> g <sup>-1</sup> )	CNF yield (g of C per g of catalyst)	Average width (nm)	D-Spacing (nm)	Surface area (m <sup>2</sup> g <sup>-1</sup> )
Ni <sub>x</sub> Cu <sub>y</sub> Mg <sub>z</sub> O	CH <sub>4</sub>	72 000	381	38	0.3389	216
Cu–Fe	CO/H <sub>2</sub> (4:1)	240 000	42	110	0.3359	76

induced by the presence of iron.<sup>173</sup> Fe was observed to have a strong interaction, whereas Cu has a weak interaction with graphite. Therefore, Fe will tend to segregate towards the solid carbon interface, as shown in Fig. 9. Besides Fe, non-iron group metal catalysts were also examined; Takenaka et al. 145 reported that adding palladium into Ni/SiO2 significantly improved the degree of precursor decomposition, because the bimetallic catalyst of Ni and Pd increased the catalytic life during the reactions.

Another bimetallic catalyst system, Fe-Ni, reported by Tananka et al., 174 showed that highly crystalline nanofibers with a controlled structure can be prepared. The structure of alignment and degree of graphitization of graphene sheets can be governed by the nature of the catalyst particles.<sup>175</sup> In the Fe-Ni bimetallic system, 174 the shape of the catalysts can greatly affect the structure of CNFs. SEM photographs illustrate that Fe-Ni is on the top of the CNFs, and in the end the CNF's structure reflects the shape of the catalysts, as shown in Fig. 10. In Fig. 10, the catalyst particles can be observed on top of highly graphitized CNFs, and the diameter of the catalyst particles is a little larger than that of the fiber. Upon increasing the temperature, the hexagonal alignment changes from platelet to tubular. In this bimetallic system, the shape of the catalyst particles can greatly affect the structure of the CNFs. However, the mechanism of how the shape changes (from platelet to tubular) is still unknown. Questions such as why the final shape of these fibers is tubular and how the chemical bonds inside them break and reconnect during the shape change remain unanswered and thus call for future research.

Besides these bimetallic catalyst systems, some groups studied multi-metallic catalysts. For example, Wang et al.176 reported a multi-metallic catalyst system to produce CNFs. In their report, as shown in Table 4, Ni, Cu, and MgO were reported to maintain their high activity for the decomposition of methane for a long time. CNFs with a platelet structure were observed by TEM. Typically, the formation of CNFs with Ni-Cu-MgO, with CH<sub>4</sub> as the carbon precursor, always led to the "herringbone" structure, while the formation of the "platelet" structure was generally observed when using CO/H2 as the precursor with an Fe-containing catalyst. As reported by Baker et al., 177 the hydrocarbon is first adsorbed on a metal crystallographic face that favors C=C bond rupture, and then the surface carbon species dissolve and diffuse through the bulk and form the graphene layers. Under the operating conditions of CO/H2 and an Fe-containing catalyst, these processes tend to proceed in a symmetrical fashion, thus leading to the formation of CNFs in a relatively straight structure, while with Ni-Cu-MgO, as reported by Haiyou's group, metal particles with

specific crystallographic orientations were generated in the reaction between CO/H2 and the Ni-Cu-MgO system, thus leading to the formation of graphite sheets that are aligned in a direction perpendicular to the longitudinal axis of the fibers. Compared with bimetallic catalyst systems, multi-metallic catalysts are active much longer at high temperatures, and the yields are much higher than those of bimetallic catalyst systems. The width of 'platelet' CNFs produced by the multimetallic catalyst is much smaller than that produced by the bimetallic catalyst system, and the inside structure of the new CNFs is much closer to that of conventional ones, which could also explain the larger surface area of the new CNFs. Moreover, the van der Waals forces decrease as the width of the structures decreases, thus leading to the increase of spacing between adjacent graphite lavers.

To conclude, the advantages of multi-metallic catalyst systems can be summarized as follows: (i) the degree of precursor decomposition and the yield of carbon materials produced are greatly improved, (ii) the structure of CNFs can be affected by the catalysts applied in the reactions; in some cases, the shape of catalyst particles can lead to the growth of CNFs in certain shapes, (iii) the stability of multi-metallic catalysts is improved thus leading to a higher yield of carbon products generated, and (iv) the morphology of CNFs can be adjusted by manipulating the catalyst particle size and composition, and the substrates used to support the catalysts.

3.2.2 Particle size effect. The characteristics of CNFs and CNTs can be affected by the catalyst particle size as well. 178,179 As discussed previously, if the catalyst particle size is extremely small, it may affect the nucleation of graphite, and thus produce amorphous carbon species. Initially, this issue was discovered in the synthesis of carbon nanotubes using the CCVD method. Yiming et al.178 studied the growth of single-walled CNTs (SWCNTs) using various sizes of particles and reported that the catalyst particle size can play a critical role in its catalytic activity in the production of CNTs. For example, the smaller particles (less than 1.8 nm) tended to be more active than larger catalyst particles (more than 7 nm) in producing SWCNTs, and SWCNTs could not be produced by the catalyst when its particle size was around 5 to 6 nm. Another paper<sup>180</sup> reported that the optimal size of catalyst particles is in the range 20 to 80 nm. If the particle size is below 10 nm, the catalyst particles may become encapsulated in the carbon shells.

There still exist some controversies about the catalyst particle size and its effect on the diameters of produced CNTs, which is attributed to different synthesis conditions. However, it is certain that if the particle size of a catalyst is below a certain size, the growth of CNTs will be blocked, and in an optimal

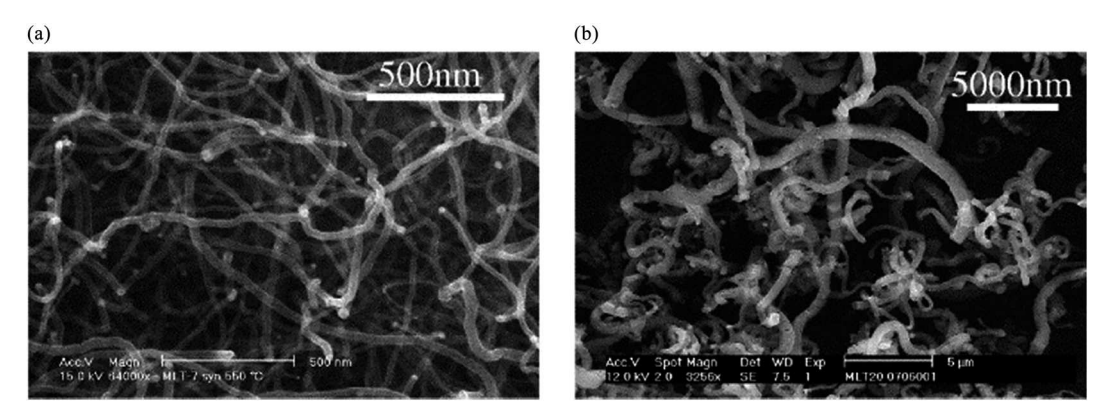


Fig. 11 (a) SEM image of CNFs grown using Ni/SiO<sub>2</sub> catalysts (b) SEM image of CNFs grown using unsupported Ni catalysts<sup>183</sup> [reproduced with permission from ELSEVIER. Copyright ELSEVIER 2002].

range of the particle size, the growth of CNTs will be accelerated with decreasing particle size. This might be because as the particle size decreases, the fiber curvature increases, which leads to an increase of strain on the basal planes of the graphite layers181 and, eventually, the formed CNTs.

More recently, it has been found that the particle size and distribution of a catalyst has an even greater influence on CNFs compared to CNTs, 131,182 because the stacking patterns of graphene layers in CNFs vary widely. Their spatial structures can be rolling, twisting, wounding, and stacking, whereas the spatial structure of CNTs is much simpler - most CNTs are formed by rolling graphene layers. Thus, this complexity of spatial structures leads to a more diverse relationship between the catalyst particle size and the structure of CNFs. Toebes et al. 183 working with CO/H<sub>2</sub> as the carbon-containing gas and SiO<sub>2</sub>-supported Ni catalysts, obtained uniform and small diameter (25 nm) CNFs, as shown in Fig. 11(a). For C<sub>2</sub>H<sub>4</sub>/H<sub>2</sub> as the carbon-containing gas and unsupported Ni catalysts, they obtained largediameter (50-500 nm) CNFs, as shown in Fig. 11(b). From SEM, no large metal particles could be found. This is because the growth of fibers continued along with the formation of a fresh metal surface. This process was terminated when no fresh metal surface was formed.

Marjolein's group also compared the effect of the catalyst particle size on nucleation and fiber formation. With small nickel particles, the nucleation and fiber formation could not be correlated with the rate of hydrocarbon decomposition, for which encapsulation happens. In contrast, with large-size particles, the growth process remains at a high level for a comparatively long time, suggesting that the fiber formation rate may remain the same as that of the hydrocarbon decomposition, and the diffusion path of the carbon units is the shortest.

The morphology of CNFs produced also depends on the concentration of catalyst particles. Tzeng et al. 184 reported, for a widely distributed catalyst in high concentration, that the diameter of the produced CNFs was large and their diameter distribution was wide, as shown in Fig. 12. The CNFs generated over an activated-carbon-fiber (ACF) substrate had diameters ranging from 20 to 30 nm. With the increased concentration of catalyst particles, the CNFs had diameters ranging from 50 to 70 nm over the ACF substrate and the CNFs had diameters ranging from 40 to 50 nm over the ACF\*A substrate. In addition, Ermakova et al.152 indicated that the concentration change of a certain catalyst in a multi-metallic catalyst system may affect the carbon yield in the reaction. Ermakova's group measured the relationship between the concentration of Ni in the Ni/SiO<sub>2</sub> catalyst and the carbon yield, and found that the highest carbon yield was 145 g per gram of catalyst when the Ni catalyst concentration reached 90% of a designed bimetallic catalyst

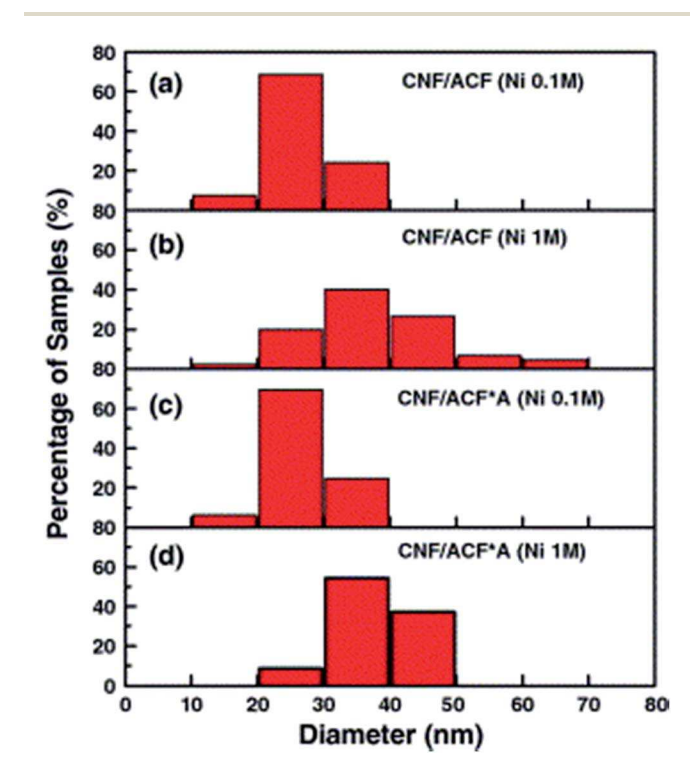


Fig. 12 Diameter distributions of carbon nanofibers grown on activated carbon fiber fabrics: (a) catalyst concentration 0.1 M, as-grown, (b) catalyst concentration 1 M, as-grown, (c) catalyst concentration 0.1 M, after acid treatment, and (d) catalyst concentration 1 M, after acid treatment<sup>184</sup> [reproduced with permission from ELSEVIER. Copyright ELSEVIER 2006].

system (90% Ni-10% Al<sub>2</sub>O<sub>3</sub>). As the concentration of Ni added to the bimetallic catalyst increased, the carbon yield constantly increased until the Ni concentration reached about 90% of the alloy catalyst. When the Ni concentration reached 100% (now the catalyst becomes a single Ni catalyst), the carbon yield showed a sharp decrease to less than 10%.

Typically, small-diameter CNFs have high surface areas and high mesopore volumes. As reported by Toebes et al. 183 smalldiameter CNFs can be produced when the particle size of a catalyst is small. Their group also found that CNFs with larger diameters are very heterogeneous and form fishbone structures in highly graphitic ordering, or less ordered platelet and some helical structures. 185,186 Thus, we can conclude that the catalyst particle size and its concentration can affect not only the yield of carbon products but also the structure of CNFs produced.

3.2.3 Catalyst stability. The catalyst stability is another key factor. 187,188 A good catalyst should extend its lifetime as long as possible so that it can lower the cost and enhance the carbon feedstock conversion as much as possible. Previous studies indicated that various parameters can affect the stability of catalysts. 189,190 Most research was focused on the temperature effects and the quality score change of catalysts, a major index that reflects the stability and the lifetime of a catalyst, precursor conversion, and carbon yield. Avdeeva et al. 191 studied Co catalysts and observed different impacts on methane conversion, lifetime of catalysts, and carbon yield. Their results are shown in Table 5. It is clearly shown that when the quality score of the Co catalysts increased from 50% to 75%, the highest precursor conversion rate decreased from 12% to 7%, the longest catalyst lifetime of the catalysts increased from 9 hours to 15 hours, and the largest carbon yield increased from 42 to 63 g per g of catalyst.

Two factors were observed. For different substrates, the impact of the Co-based catalysts on precursor decomposition was different. For example, under the same quality score (50 wt% Co), the methane conversion rate of Co-Al<sub>2</sub>O<sub>3</sub> was more than twice that of Co-MgO. Another factor is that when the reaction temperature was relatively low, in some cases, the catalyst was not even activated, which explained the low activity of 75 wt% Co-MgO in the reaction.

Chai et al. 192 reached a different conclusion. In their investigation, the methane conversion decreased when the quality score increased. Under the same quality score, the conversion of methane on aluminium oxides was higher than those on the

Table 5 Catalytic properties of Co-based catalysts on methane decomposition (reaction temperature: 500 °C)191

Catalysts	Methane conversion (%)	Lifetime (h)	Carbon yield $(g_C g_{Co}^{-1})$
50 wt% Co-MgO	5.5	3	7.3
50 wt% Co-SiO <sub>2</sub>	7	9	22
50 wt% Co-Al <sub>2</sub> O <sub>3</sub>	12	8	42
75 wt% Co-MgO	0	0	0
75 wt% Co-SiO <sub>2</sub>	7	4	11
75 wt% Co–Al $_2$ O $_3$	7	15	63

other oxides; below 70 wt%, the aluminium oxide-based catalysts showed the longest lifetime. The methane conversion decreased with increasing temperature. Another detailed study was conducted by Avdeeva et al.193 for the lifetime of 85% Fe-5%-Al<sub>2</sub>O<sub>3</sub> in the relatively moderate temperature range from 600 to 675 °C at intervals of 25 °C. Their results indicated that when the temperature was increased to 625 °C, the catalyst lifetime reached its peak (16.5 hours) and the carbon yield reached its peak (16 g per 1 g of catalyst). Meanwhile, when the temperature was continuously increased, the lifetime of the catalyst and the carbon yield began to decrease. Eventually, the lifetime of the catalyst remained almost the same as that at the initial temperature (600 °C) when temperature reached its peak (675 °C), while the precursor conversion increased with temperature.

In some cases, mixtures of metal catalysts showed a better stability than a single catalyst. The reason for this could be that, at the early stage of the reaction, the basic sites are relatively few at the particle surface. As the reaction continues, a balance between the generation of carbon and its bulk diffusion through the particle can be reached. However, when it comes to bimetallic catalyst systems, the active metal was exposed rapidly, and the rate of generation of carbon was much slower than the diffusion rate, which made carbon encapsulate the particle and deactivate the catalyst. 176 Dussault et al. 194 reported that a small amount of Cu (less than 10 wt%) promoted the activity and the stability of Ni-Mg-Al catalysts in the CCVD reaction, but the addition of a large amount of Cu significantly reduced the activity of the catalyst and thus the CNF yields. This is mainly because the small amount of Cu contributes to the diffusion of hydrogen thus inhibiting the formation of encapsulating coke.195 Monzon et al.196 pointed out that, from the perspective of kinetics, the Ni-Mg-Al catalyst system suffered deactivation by coke formation at low temperatures while that with a small amount of Cu (less than 20 wt%) could promote the stability and activity of the Al-Ni based multi-metallic catalyst system. While the quality score of Cu increased, the carbon yield showed a sharp decrease, as shown in Fig. 13.

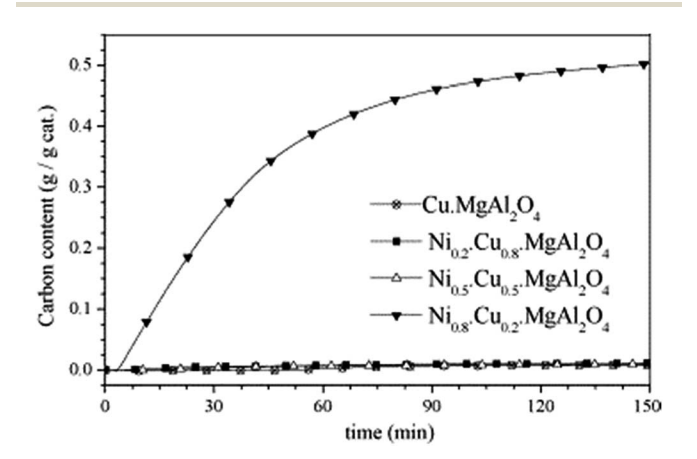


Fig. 13 Evolution with time of the carbon content for different Ni-Cu catalysts. Reaction temperature, 700 °C; feed composition, 5% CH<sub>4</sub>/ 95% N<sub>2</sub> (ref. 196) [reproduced with permission from ELSEVIER. Copyright ELSEVIER 2006].

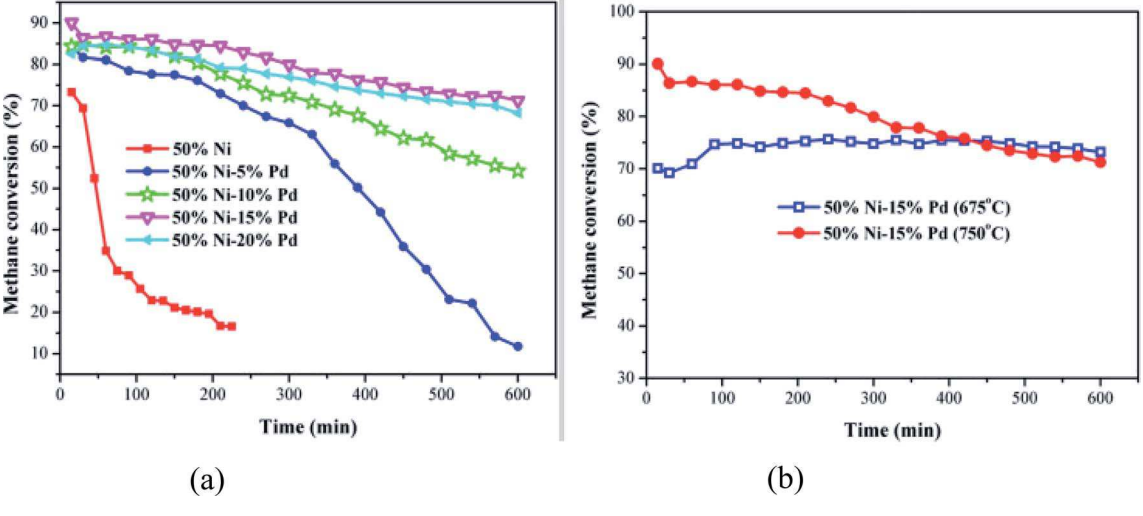


Fig. 14 (a) Stability of the 50% Ni/Al<sub>2</sub>O<sub>3</sub> and 50% Ni–Pd/Al<sub>2</sub>O<sub>3</sub> catalysts with various palladium loadings at 750 °C (b) stability of the 50% Ni–15% Pd/Al<sub>2</sub>O<sub>3</sub> catalyst at different reaction temperatures<sup>197</sup> [reproduced with permission from ELSEVIER. Copyright ELSEVIER 2016].

Bayat et al. 197 reported a new synthesis route with simultaneous production of CO<sub>x</sub>-free hydrogen and CNFs using Nibased alloy catalysts. They innovatively added palladium to nickel catalysts (Ni-Pd catalyst) that enhanced the carbon precursor dissociation and increased the catalytic activity. In the experiment, they found that 50% Ni-15% Pd/Al<sub>2</sub>O<sub>3</sub> catalysts showed a promising catalyst lifetime, as shown in Fig. 14. Fig. 14(a) clearly shows that with a little addition of palladium (5%), the catalyst lifetime increased significantly. This can be attributed to the relatively higher ability of palladium to transfer carbon, compared to a single Ni catalyst. 145 Moreover, as reported by Takenaka et al., 198 CNFs grew from several facets in a Pd-containing catalyst system and formed branched

structures during methane decomposition. Nishiyama et al. 195 also evidenced this fact that Pd alloy particles formed CNFs from several facets, at the initial stage of the reaction, compared to the single Pd catalyst, which formed CNFs from only one facet. This multi-faceted growth of CNFs increases the rate of carbon migration and prevents the coverage of active sites, thus leading to Pd-containing catalysts displaying a higher activity and longer life for methane decomposition. When the percentage of palladium reached 15%, however, the catalyst lifetime did not show an obvious enhancement. Increasing the palladium concentration decreased the surface area and thus limited the carbon diffusion.199

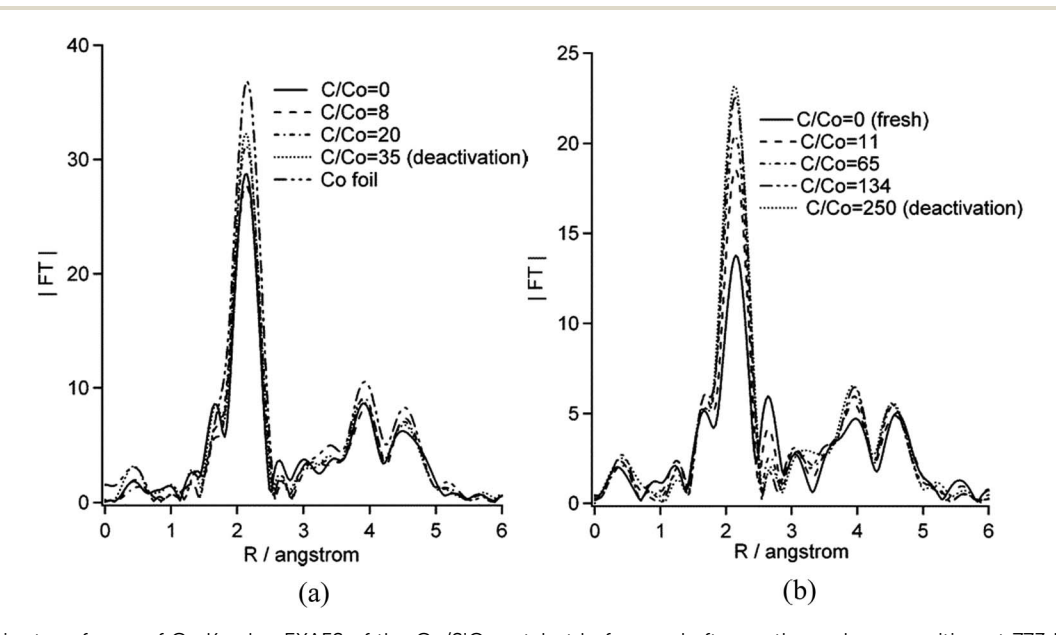


Fig. 15 (a) Fourier transforms of Co K-edge EXAFS of the Co/SiO<sub>2</sub> catalyst before and after methane decomposition at 773 K and of Co foil. Loading of Co = 5 wt% (b) Fourier transforms of Co K-edge EXAFS of the  $Co/Al_2O_3$  catalyst before and after methane decomposition at 773 K and of Co foil. Loading of Co = 5 wt% (ref. 205) [reproduced with permission from ELSEVIER. Copyright ELSEVIER 2004].

As can be seen from Fig. 14(b), temperature also plays an important role in the catalytic process. Since this process is an endothermic reaction, higher temperatures can accelerate carbon diffusion through the bulk, thus leading to a higher rate of carbon graphene layer formation. Therefore, the methane conversion is much higher at higher temperatures at an early stage of the reaction. This is because higher temperatures generate quasi-liquid and fragmented nickel particles that are encapsulated within the carbon fibers.200 However, as the reaction proceeds, the methane higher-temperature conversion decreases while lower-temperature conversion increases. This is because a higher temperature transforms the Pd-Ni catalyst into its quasi-liquid state, and catalysts in this state tend to be smaller in size than in their metallic state. A small-size catalyst

can be encapsulated by carbon layers, thus decreasing the rate of CNF formation and causing lower methane conversion. As reported by Chen et al.,205 the quasi-liquid state of catalyst particles can be vulnerable to splitting into small pieces and thus become encapsulated in the carbon layers. Furthermore, this process causes the rate of carbon diffusion to be higher than the rate of fiber formation, and carbon starts to accumulate on the metal surfaces, thus leading to catalyst deactivation.

3.2.4 Catalyst support effect. Support substrates can physically and chemically affect the catalyst particle size and its distribution. 202,203 Physically, substrates with different morphologies, such as power, liquid, or small solid particles, may hold the catalysts in place and control the size of metal catalyst particles during the synthesis and reaction. Chemically,

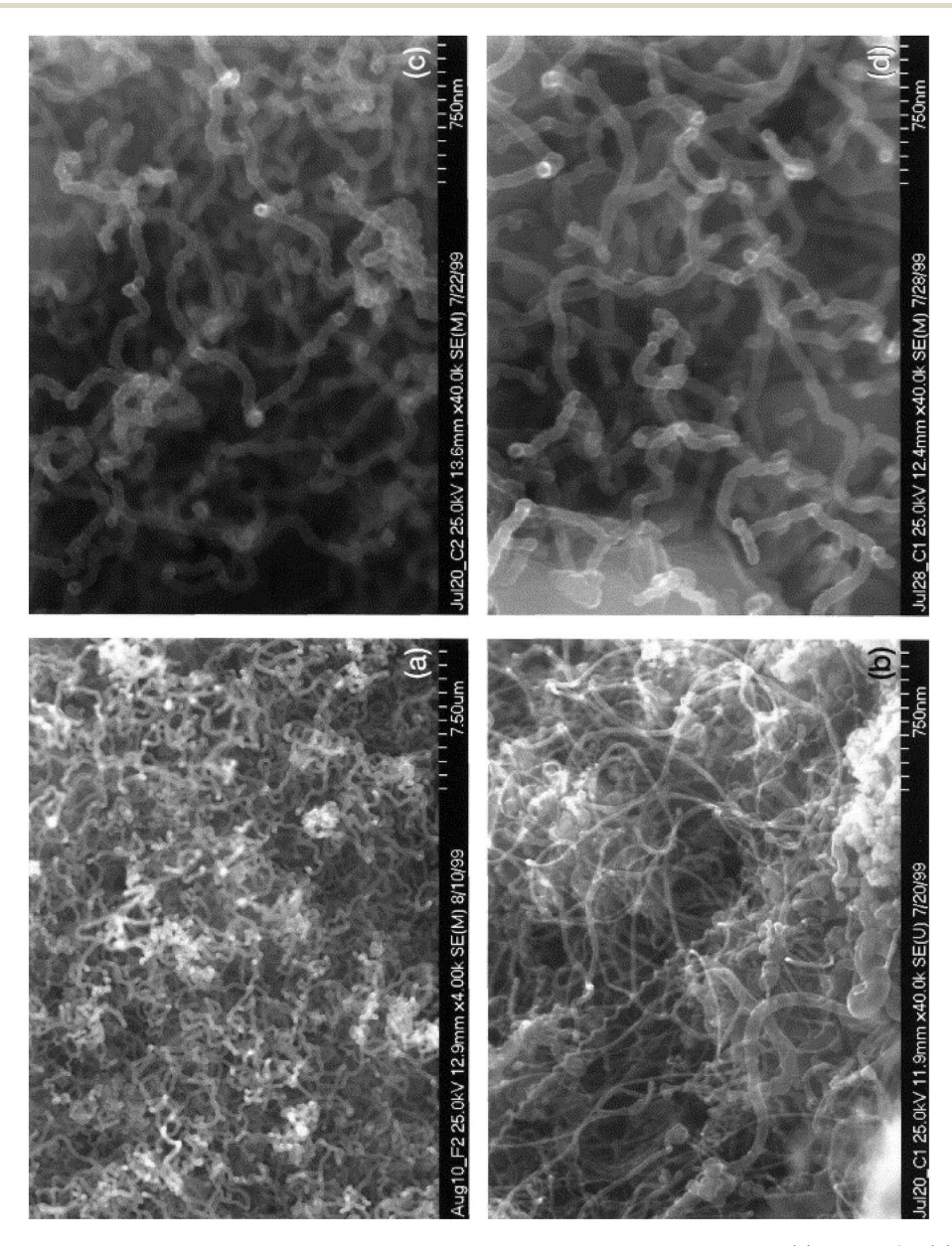


Fig. 16 SEM images of catalytically synthesized carbon nanofibers. The metal-support systems used are (a) Ni on TiO<sub>2</sub>; (b) Fe on CaO; (c) Cu on CaO; and (d) Cu on SiO<sub>2</sub> (ref. 204) [reproduced with permission from American Chemical Society. Copyright American Chemical Society 2004].

the substrates may act as a source that assists metal catalyst particles gaining negative charge, which could, to a certain degree, enhance the metal-catalyst activity.204

Takenaka et al. 201,204 investigated the catalytic performance of Co supported on different oxide supports (MgO, Al<sub>2</sub>O<sub>3</sub>, SiO<sub>2</sub> and TiO<sub>2</sub>) for the decomposition of methane at 773 K in synthesizing CNFs. They concluded that the catalytic performance of Co/ Al<sub>2</sub>O<sub>3</sub> and Co/MgO was superior to those of Co/TiO<sub>2</sub> and Co/ SiO<sub>2</sub>. From the Fourier transforms of Co K-edge EXAFS of Co/ Al<sub>2</sub>O<sub>3</sub> and Co/SiO<sub>2</sub>, shown in Fig. 15, the group concluded that the average crystallite size of Co/Al<sub>2</sub>O<sub>3</sub> is smaller than that of Co/ SiO<sub>2</sub>, and, with smaller particle size, the methane decomposition is more effective. This is mainly because the deactivation rate of Co on the SiO2 substrate is much smaller than that on the Al<sub>2</sub>O<sub>3</sub> substrate.

Vander Wal et al. 203 compared the CNF growth on Al<sub>2</sub>O<sub>3</sub>, CaO, SiO<sub>2</sub>, and TiO<sub>2</sub> substrates using iron-group catalysts. Assuming CNTs to be one type of CNFs, they found that Ni over TiO<sub>2</sub> displayed the highest fiber yield among all substrates, as illustrated in Fig. 16(a). Ni over CaO showed the lowest catalytic activities, while Cu was the most active on CaO and SiO2, as illustrated in Fig. 16(c) and (d). Fe showed high activity over the CaO substrate, as illustrated in Fig. 16(b). Even though, in most cases, the catalyst particle sizes are roughly the same, there are huge differences in the fiber yields and structures of CNFs. de Los Arcos et al. 206 and Kanzow et al. 207 reported that, in a diffusion-based model of growth, the surface area between the catalyst particles and substrates provided a region for the precipitation of carbon atoms to take place, and the growth rate would be slower when the contact area was reduced.

Zhao et al.208 studied the interaction between metal catalyst particles and substrates from the perspective of classical molecular dynamics. In their study, a catalyst/substrate system was simulated by fixing one layer of metal clusters on a hard wall (substrate), as shown in Fig. 17. Their results indicated that the interaction reduced the cluster melting point, thus reducing the solubility of carbon atoms inside the metal particles. In favor of the model proposed by Zhao et al., Homma et al.<sup>209</sup> also found that Fe and Co exhibited a melting point drop on the SiO<sub>2</sub> substrate during the CCVD reaction. They also found that the reaction between the metallic particles and the substrate favored the growth of CNFs or CNTs and, in some cases, the substrate may have caused catalyst poisoning, in which silicide formation deactivated the Fe and Co catalysis.

In the following years, Mattevi et al. strengthened this 'metal-support' theory.210 In their study, in situ X-ray photoelectron spectroscopy was used to observe the interaction between an Fe catalyst and Al<sub>2</sub>O<sub>3</sub>, and the Fe catalyst and SiO<sub>2</sub>. Their results suggest that the Al<sub>2</sub>O<sub>3</sub> support promotes CNT yield in the CCVD reaction because the formation of Fe<sup>2+</sup> and Fe<sup>3+</sup> on Al<sub>2</sub>O<sub>3</sub> restricts the Fe surface mobility, reduces the range of catalyst particle size distribution, and thus contributes to the nucleation of CNTs.

All in all, the supporting substrate can significantly impact the catalyst performance.211,212 The characteristics of catalyst supports can determine the properties of the CNFs or other carbon materials produced by the reaction with metallic catalyst particles. The experimental data and theories aimed at explaining them can be controversial, and thus call for more research.

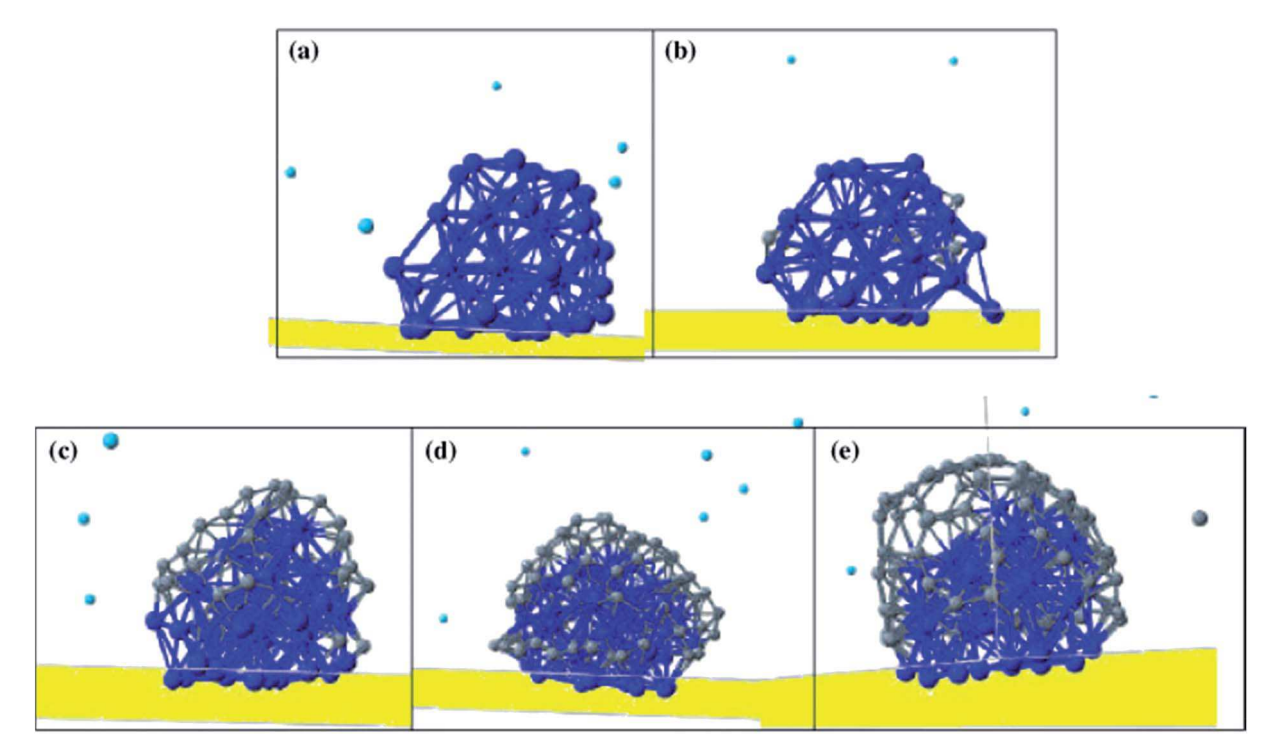


Fig. 17 Molecular dynamics simulations of nanotube growth from a precursor gas (light blue spheres) at 1023 K on a Ni<sub>48</sub> nanocluster: 11 Ni atoms are fixed to the hard wall (yellow), 37 are free. After the reaction, the precursor gas is transformed into C atoms (grey spheres)<sup>208</sup> [reproduced with permission from IOP Publishing Ltd. Copyright IOP Publishing Ltd 2005]

### 4. Summary and outlook

The most recent progress made in the catalytic synthesis of CNFs is reviewed from the perspective of catalyst characteristics and their interactions with the supporting substrate and carbon precursors. The characteristics of catalysts, including their composition, particle sizes, and stabilities, the type of catalyst support, and the type of carbon precursor all contribute significantly to the quality of the produced CNFs. As for the mechanism of the catalytic growth of CNFs, the decomposition of the carbon precursor and the diffusion of carbon atoms into metal particle clusters are considered to be the key processes determining the growth of CNFs.

However, much more work is needed to produce CNFs catalytically. For example, the challenge is how to scale up the lab-demonstrated CNF synthesis. Furthermore, better precursors for synthesizing functionalized CNFs need to be engineered. Also, high-performance and high-stability catalysts are needed for the synthesis of cost-effective CNFs. Finally, far more advanced theoretical work, including molecular simulation, is needed to understand the properties of new CNFs, and how they are related to the synthesis conditions.

### Acknowledgements

The authors gratefully express their thanks to the National Science Foundation (NSF OIA-1632899) in the U.S., DOE (DE-FE0023999) and Idaho National Laboratory (Laboratory Directed Research and Development Program) under DOE Idaho Operations Office Contract DE-AC07-05ID14517 for partial support to this research.

#### References

- X. J. Yang, D. Austin, M. A. Guillorn, V. I. Merkulov,
   A. V. Melechko, D. H. Lowndes and M. L. Simpson,
   Nanotechnology, 2003, 3, 342–345.
- 2 A. Parish, *Production and application of carbon nanotubes, carbon nanofibers, fullerenes, graphene and nanodiamonds: a global technology survey and market analysis*, Innovative Research and Products Inc., 2011.
- 3 K. P. De Jong and J. W. Geus, Catal. Rev., 2000, 42, 481-510.
- 4 S. A. Freunberger, Y. Chen, Z. Peng, J. M. Griffin, L. J. Hardwick, F. Barde, P. Novak and P. G. Bruce, *J. Am. Chem. Soc.*, 2011, **133**, 8040–8047.
- 5 M. M. Ottakam Thotiyl, S. A. Freunberger, Z. Peng and P. G. Bruce, J. Am. Chem. Soc., 2013, 135, 494–500.
- 6 R. R. Mitchell, B. M. Gallant, C. V. Thompson and Y. Shao-Horn, *Energy Environ. Sci.*, 2011, 4, 2952.
- 7 E. J. Ra, E. Raymundo-Piñero, Y. H. Lee and F. Béguin, Carbon, 2009, 47, 2984–2992.
- 8 S. H. Park, S. B. Yoon, H. K. Kim, J. T. Han, H. W. Park, J. Han, S. M. Yun, H. G. Jeong, K. C. Roh and K. B. Kim, *Sci. Rep.*, 2014, 4, 6118.
- 9 P. J. Lamas-Ardisana, P. Fanjul-Bolado and A. Costa-García, J. Electroanal. Chem., 2016, 775, 129–134.

- 10 L. Zhou, P. Fu, X. Cai, S. Zhou and Y. Yuan, *Appl. Catal., B*, 2016, **188**, 31–38.
- 11 Y. Wang and M. Shahvali, Fuel, 2016, 163, 65-73.
- 12 F. Han, G. Meng, F. Zhou, L. Song, X. Li, X. Hu, X. Zhu, B. Wu and B. Wei, *Sci. Adv.*, 2015, 1, e1500605.
- 13 M. Cakici, R. R. Kakarla and F. Alonso-Marroquin, *Chem. Eng. J.*, 2017, 309, 151–158.
- 14 S. H. Yoon, S. Lim, S. H. Hong, W. M. Qiao, D. D. Whitehurst, I. Mochida, B. An and K. Yokogawa, *Carbon*, 2005, 43, 1828–1838.
- 15 Y. Kong, X. D. Shen, S. Cui and M. H. Fan, *RSC Adv.*, 2014, 4, 64193–64199.
- 16 R. Chu, W. Hou, X. Meng, T. Xu, Z. Miao, G. Wu and L. Bai, Chin. J. Chem. Eng., 2016, 24, 1735–1741.
- 17 J. Kong, A. M. Cassell and H. J. Dai, Chem. Phys. Lett., 1998, 292, 567–574.
- 18 G. Che, B. B. Lakshmi, C. R. Martin, E. R. Fisher and R. S. Ruoff, *Chem. Mater.*, 1998, **10**, 260–267.
- 19 S. Hofmann, C. Ducati, J. Robertson and B. Kleinsorge, *Appl. Phys. Lett.*, 2003, **83**, 135–137.
- 20 A. Oberlin, M. Endo and T. Koyama, *J. Cryst. Growth*, 1976, 32, 335–349.
- 21 N. M. Rodriguez, A. Chambers and R. T. K. Baker, *Langmuir*, 1995, **11**, 3862–3866.
- 22 S. B. Sinnott, R. Andrews, D. Qian, A. M. Rao, Z. Mao, E. C. Dickey and F. Derbyshire, *Chem. Phys. Lett.*, 1999, 315, 25–30.
- 23 B. Zhang, F. Kang, J.-M. Tarascon and J.-K. Kim, *Prog. Mater. Sci.*, 2016, 76, 319–380.
- 24 H. Kim, Y. Kim, J. Kim and W. Y. Kim, *Carbon*, 2016, 98, 404–410.
- 25 M. Hassan, K. R. Reddy, E. Hague, A. I. Minett and V. G. Gomes, *J. Colloid Interface Sci.*, 2013, **410**, 43–51.
- 26 M. U. Khan, K. R. Reddy, T. Snguanwongchai, E. Haque and V. G. Gomes, *Colloid Polym. Sci.*, 2016, 294, 1599–1610.
- 27 K. R. Reddy, B. C. Sin, C. H. Yoo, D. Sohn and Y. Lee, *J. Colloid Interface Sci.*, 2009, **340**, 160–165.
- 28 K. R. Reddy, H. M. Jeong, Y. Lee and A. V. Raghu, *J. Polym. Sci., Part A: Polym. Chem.*, 2010, **48**, 1477–1484.
- 29 M. Hassan, E. Haque, K. R. Reddy, A. I. Minett, J. Chen and V. G. Gomes, *Nanoscale*, 2014, 6, 11988–11994.
- 30 K. R. Reddy, B. C. Sin, K. S. Ryu, J. Noh and Y. Lee, *Synth. Met.*, 2009, **159**, 1934–1939.
- 31 S. H. Choi, D. H. Kim, A. V. Raghu, K. R. Reddy, H. I. Lee, K. S. Yoon, H. M. Jeong and B. K. Kim, *J. Macromol. Sci.*, Part B: Phys., 2012, 51, 197–207.
- 32 D. R. Son, A. V. Raghu, K. R. Reddy and H. M. Jeong, *J. Macromol. Sci., Part B: Phys.*, 2016, 55, 1099–1110.
- 33 J. W. Snoeck, G. F. Froment and M. Fowles, *J. Catal.*, 1997, **169**, 240–249.
- 34 I. Martin-Gullon, J. Vera, J. A. Conesa, J. L. González and C. Merino, *Carbon*, 2006, 44, 1572–1580.
- 35 L. Wei and G. Yushin, Nano Energy, 2012, 1, 552-565.
- 36 W.-J. Youe, S.-M. Lee, S.-S. Lee, S.-H. Lee and Y. S. Kim, *Int. J. Biol. Macromol.*, 2016, **82**, 497–504.
- 37 L. Bai, Karnowo, S. Kudo, K. Norinaga, Y. G. Wang and J. Hayashi, *Energy Fuels*, 2014, **28**, 7133–7139.

- 38 Y. Kong, G. Jiang, M. Fan, X. Shen, S. Cui and A. G. Russell, *Chem. Commun.*, 2014, **50**, 12158–12161.
- 39 G. G. Stavropoulos and A. A. Zabaniotou, *Fuel Process*. *Technol.*, 2009, **90**, 952–957.
- 40 Y. G. Wang, J. L. Zhou, L. Bai, Y. J. Chen, S. Zhang and X. C. Lin, *Energy Fuels*, 2014, 28, 862–867.
- 41 X.-q. Xu, Y.-g. Wang, Z.-d. Chen, L. Bai, K.-j. Zhang, S.-s. Yang and S. Zhang, *J. Fuel Chem. Technol.*, 2015, 43, 1–8.
- 42 X.-q. Xu, Y.-g. Wang, Z.-d. Chen, X.-j. Chen, H.-y. Zhang, L. Bai and S. Zhang, *J. Anal. Appl. Pyrolysis*, 2015, 115, 233–241.
- 43 Q. Liu, C. Lv, Y. Yang, F. He and L. Ling, *J. Mol. Struct.*, 2005, 733, 193–202.
- 44 B. Hu, K. Wang, L. H. Wu, S. H. Yu, M. Antonietti and M. M. Titirici, Adv. Mater., 2010, 22, 813–828.
- 45 M. Endo, T. Koyama and Y. Hishiyama, *Jpn. J. Appl. Phys.*, 1976, **15**, 2073–2076.
- 46 E. Fitzer, W. Hüttner and L. M. Manocha, *Carbon*, 1980, 18, 291–295.
- 47 F. Benissad, P. Gadelle, M. Coulon and L. Bonnetain, *Carbon*, 1988, **26**, 425–432.
- 48 G. G. Tibbetts, J. Cryst. Growth, 1984, 66, 632-638.
- 49 S. Lijima, Nature, 1991, 354, 56-58.
- 50 A. G. Rinzler, J. Liu, H. Dai, P. Nikolaev, C. B. Huffman, F. J. Rodriguez-Macias, P. J. Boul, A. H. Lu, D. Heymann, D. T. Colbert, R. S. Lee, J. E. Fischer, A. M. Rao, P. C. Eklund and R. E. Smalley, *Appl. Phys. A: Mater. Sci. Process.*, 1998, 67, 29–37.
- 51 C. Kim, K. S. Yang, M. Kojima, K. Yoshida, Y. J. Kim, Y. A. Kim and M. Endo, *Adv. Funct. Mater.*, 2006, 16, 2393–2397.
- 52 K. R. Reddy, V. G. Gomes and M. Hassan, *Mater. Res. Express*, 2014, 1, 1.
- 53 E. X. Ding, H. Z. Geng, J. Wang, Z. J. Luo, G. F. Li, W. Y. Wang, L. G. Li, H. J. Yang, S. X. Da, J. Wang, H. Jiang and E. I. Kauppinen, *Nanotechnology*, 2016, 27, 085602.
- 54 K. R. Reddy, B. C. Sin, C. H. Yoo, W. J. Park, K. S. Ryu, J. S. Lee, D. W. Sohn and Y. I. Lee, *Scr. Mater.*, 2008, 58, 1010–1013.
- 55 T. W. Ebbesen, *Carbon Nanotubes: Preparation and Properties*, CRC Press, Boca Raton, 1997.
- 56 M. Su, B. Zheng and J. Liu, *Chem. Phys. Lett.*, 2000, **322**, 321–326.
- 57 F. Ko, Y. Gogotsi, A. Ali, N. Naguib, H. Ye, G. L. Yang, C. Li and P. Willis, *Adv. Mater.*, 2003, **15**, 1161–1165.
- 58 A. L. Yarin, *Introduction to Electrospinning and Nanofibers*, World Scientific, 2005.
- 59 C. J. Angammana and S. H. Jayaram, *Part. Sci. Technol.*, 2016, 34, 72–82.
- 60 W. E. Teo and S. Ramakrishna, *Nanotechnology*, 2006, 17, R89–R106.
- 61 M. M. Hohman, M. Shin, G. Rutledge and M. P. Brenner, *Phys. Fluids*, 2001, **13**, 2201–2220.
- 62 Y. M. Shin, M. M. Hohman, M. P. Brenner and G. C. Rutledge, *Appl. Phys. Lett.*, 2001, **78**, 1149–1151.

- 63 D. H. Reneker, A. L. Yarin, H. Fong and S. Koombhongse, J. Appl. Phys., 2000, 87, 4531–4547.
- 64 F. Tourlomousis, H. Z. Ding, A. Dole and R. C. Chang, Proceedings of the Asme 11th International Manufacturing Science and Engineering Conference, 2016, p. 2.
- 65 G. Allaedini, S. M. Tasirin and P. Aminayi, *Diamond Relat. Mater.*, 2016, 66, 196–205.
- 66 Y. Liu, J. Luo, C. Helleu, M. Behr, H. Ba, T. Romero, A. Hébraud, G. Schlatter, O. Ersen, D. S. Su and C. Pham-Huu, *J. Mater. Chem. A*, 2017, 5, 2151–2162.
- 67 C. F. Powell, J. H. Oxley and J. M. Blocher, *Vapour Deposition*, The Electrochemical Society, Pennington NJ, 1966.
- 68 S. Iijima, Y. Aikawa and K. Baba, *Appl. Phys. Lett.*, 1990, 57, 2646–2648.
- 69 S. Iijima and T. Ichihashi, *Phys. Rev. Lett.*, 1986, **56**, 616–619.
- 70 J. Matsuda, K. Fukunaga and K. Ito, *Geochim. Cosmochim. Acta*, 1991, 55, 2011–2023.
- 71 W. G. Eversole, US Patent, 3030188., 1962.
- 72 P. M. Martineau, S. C. Lawson, A. J. Taylor, S. J. Quinn, D. J. F. Evans and M. J. Crowder, Gems Gemol., 2004, 40, 2–25.
- 73 T. V. Hughes and C. R. Chambers, U.S. Patent, 405480., 1889.
- 74 T. Iwasaki, Y. Makino, M. Fukukawa, H. Nakamura and S. Watano, *Appl. Nanosci.*, 2016, **6**, 1211–1218.
- 75 Y. Xie, L. Lu, Y. Tang, F. Zhang, C. Shen, X. Zang, X. Ding, W. Cai and L. Lin, *Mater. Lett.*, 2017, **186**, 70–73.
- 76 Y. Mokuno, A. Chayahara, H. Yamada and N. Tsubouchi, *Diamond Relat. Mater.*, 2009, **18**, 1258–1261.
- 77 J. Isberg, A. Lindblom, A. Tajani and D. Twitchen, *Phys. Status Solidi A*, 2005, **202**, 2194–2198.
- 78 X. Jiang, C. P. Klages, R. Zachai, M. Hartweg and H. J. Fusser, *Appl. Phys. Lett.*, 1993, **62**, 3438–3440.
- 79 J. R. Rabeau, S. T. Huntington, A. D. Greentree and S. Prawer, *Appl. Phys. Lett.*, 2005, **86**, 134104.
- 80 http://www.innovateus.net/science/what-chemical-vapor-deposition.
- 81 M. L. Bunch, J. B. Price and R. W. Stitz, U.S. Patent No. 4640224., 1987.
- 82 R. B. Simon, J. Anaya, F. Faili, R. Balmer, G. T. Williams, D. J. Twitchen and M. Kuball, *Appl. Phys. Express*, 2016, 9, 061302.
- 83 S. Yousef and A. Mohamed, *J. Mech. Sci. Technol.*, 2016, **30**, 5135–5141.
- 84 H. Windischmann, G. F. Epps, Y. Cong and R. W. Collins, *J. Appl. Phys.*, 1991, **69**, 2231–2237.
- 85 K. Fairbairn and R. Nowak, U.S. Patent No. 5614055., 1997.
- 86 K. Inoue, M. Michimori, M. Okuyama and Y. Hamakawa, *Jpn. J. Appl. Phys.*, 1987, **26**, 805–811.
- 87 V. K. Varadan and J. N. Xie, *Smart Mater. Struct.*, 2002, **11**, 610-616.
- 88 B. W. Yu, Q. K. Zhang, L. Z. Hou, S. L. Wang, M. Song, Y. H. He, H. Huang and J. Zou, *Carbon*, 2016, **96**, 904–910.
- 89 D. Kang and J. W. Lee, Appl. Catal., B, 2016, 186, 41-55.

- 90 G. Q. Wang, S. Kuang and W. Zhang, Mater. Lett., 2016, 174, 14-16.
- 91 I. T. Ghampson, C. Sepulveda, R. Garcia, J. L. G. Fierro and N. Escalona, Catal. Sci. Technol., 2016, 6, 4356-4369.
- 92 S. Cui, W. Cheng, X. Shen, M. Fan, A. Russell, Z. Wu and X. Yi, Energy Environ. Sci., 2011, 4, 2070-2074.
- 93 B. Dutcher, M. H. Fan and A. G. Russell, ACS Appl. Mater. Interfaces, 2015, 7, 2137-2148.
- 94 N. Miyajima, K. Jinguji, T. Matsumura, T. Matsubara, H. Sakane, T. Akatsu and O. Tanaike, J. Phys. Chem. Solids, 2016, 91, 122-127.
- 95 M. S. Chandran, K. Sanil, K. Sunitha, D. Mathew, V. L. Rao and C. P. R. Nair, Polym. Adv. Technol., 2016, 27, 984-992.
- 96 M. Pommet, J. Juntaro, J. Y. Y. Heng, A. Mantalaris, A. F. Lee, K. Wilson, G. Kalinka, M. S. P. Shaffer and A. Bismarck, Biomacromolecules, 2008, 9, 1643-1651.
- 97 V. K. Thakur and M. K. Thakur, Carbohydr. Polym., 2014, 109, 102-117.
- 98 L. X. Ling, M. H. Fan, B. J. Wang and R. G. Zhang, Energy Environ. Sci., 2015, 8, 3109-3133.
- 99 N. Hiremath, J. Mays and G. Bhat, Polym. Rev., 2016, 1-30.
- 100 Z. Y. Zeng and J. H. Lin, RSC Adv., 2014, 4, 40251-40258.
- 101 N. Muradov, P. Choi, F. Smith and G. Bokerman, J. Power Sources, 2010, 195, 1112-1121.
- 102 M. M. Titirici, A. Thomas, S. H. Yu, J. O. Muller and M. Antonietti, Chem. Mater., 2007, 19, 4205-4212.
- 103 B. Hu, K. Wang, L. H. Wu, S. H. Yu, M. Antonietti and M. M. Titirici, Adv. Mater., 2010, 22, 813-828.
- 104 B. Cagnon, X. Py, A. Guillot, F. Stoeckli and G. Chambat, Bioresour. Technol., 2009, 100, 292-298.
- 105 J. F. Kadla, S. Kubo, R. A. Venditti, R. D. Gilbert, A. L. Compere and W. Griffith, Carbon, 2002, 40, 2913-2920.
- 106 K. Koziol, J. Vilatela, A. Moisala, M. Motta, P. Cunniff, M. Sennett and A. Windle, Science, 2007, 318, 1892-1895.
- 107 E. Schroder, K. Thomauske, C. Weber, A. Hornung and V. Tumiatti, J. Anal. Appl. Pyrolysis, 2007, 79, 106-111.
- 108 J. F. Gonzalez, S. Roman, J. M. Encinar and G. Martinez, J. Anal. Appl. Pyrolysis, 2009, 85, 134-141.
- 109 M. MolinaSabio, M. T. Gonzalez, F. RodriguezReinoso and A. SepulvedaEscribano, Carbon, 1996, 34, 505-509.
- 110 M. MolinaSabio, F. RodriguezReinoso, F. Caturla and M. J. Selles, Carbon, 1996, 34, 457-462.
- 111 M. A. de la Casa-Lillo, J. Alcaniz-Monge, E. Raymundo-Pinero, D. Cazorla-Amoros and A. Linares-Solano, Carbon, 1998, 36, 1353-1360.
- 112 T. Horikawa, J. Hayashi and K. Muroyama, Carbon, 2002, 40, 709-714.
- 113 A. R. Mohamed, M. Mohammadi and G. N. Darzi, Renewable Sustainable Energy Rev., 2010, 14, 1591-1599.
- 114 W. M. A. W. Daud and W. S. W. Ali, Bioresour. Technol., 2004, 93, 63-69.
- 115 A. J. Tsamba, W. H. Yang and W. Blasiak, Fuel Process. Technol., 2006, 87, 523-530.
- 116 A. Demirbas, Energy Convers. Manage., 2003, 44, 1481-1486.
- 117 M. Kumar and R. C. Gupta, J. Mater. Sci. Lett., 1992, 11, 1439-1440.

- C. Tangsathitkulchai 118 Y. Ngernyen, and M. Tangsathitkulchai, Korean J. Chem. Eng., 2006, 23, 1046-1054.
- 119 M. Jagtoyen and F. Derbyshire, Carbon, 1998, 36, 1085-
- 120 M. Soleimani and T. Kaghazchi, Chem. Eng. Technol., 2007, 30, 649-654.
- 121 Y. Munoz-Gonzalez, R. Arriagada-Acuna, G. Soto-Garrido and R. Garcia-Lovera, J. Chem. Technol. Biotechnol., 2009, 84, 39-47.
- 122 B. Kaynak, H. Topal and A. T. Atimtay, Fuel Process. Technol., 2005, 86, 1175-1193.
- 123 M. Endo, Y. A. Kim, T. Hayashi, Y. Fukai, K. Oshida, Terrones, T. Yanagisawa, S. Higaki M. S. Dresselhaus, Appl. Phys. Lett., 2002, 80, 1267-1269.
- 124 J. Y. Z. Fan, T. Wei, G. Ning, L. Zhi, J. Liu, D. Cao, G. Wang and F. Wei, ACS Nano., 2011, 5, 2782-2794.
- 125 E. Edwin, B. Rusten and T. Arnesen, U.S. Patent No. 20060013757 A1, 2003.
- 126 J. Hoekstra, J. W. Geus and L. W. Jenneskens, U.S. Patent No.20120157298., 2012.
- 127 S. Hong, J. Park, J. O. Kim, J. K. Park, O. H. Keun-hwan, Y. Lee, M. Choo, H. A. Jin-su and Lees, U.S. Patent No. 20150111124., 2015.
- 128 P. Tribolet and L. Kiwi-Minsker, Catal. Today, 2005, 102, 15-22.
- 129 A. J. H. M. Kock, P. K. Debokx, E. Boellaard, W. Klop and J. W. Geus, J. Catal., 1985, 96, 468-480.
- 130 I. Alstrup, J. Catal., 1988, 109, 241-251.
- 131 G. B. Zheng, K. Kouda, H. Sano, Y. Uchiyama, Y. F. Shi and H. J. Quan, Carbon, 2004, 42, 635-640.
- 132 C. Bower, O. Zhou, W. Zhu, D. J. Werder and S. H. Jin, Appl. Phys. Lett., 2000, 77, 2767-2769.
- 133 G. Emig, N. Popovska, G. Schoch and T. Stumm, Carbon, 1998, 36, 407-415.
- 134 V. Jourdain and C. Bichara, Carbon, 2013, 58, 2-39.
- 135 A. C. Dupuis, Prog. Mater. Sci., 2005, 50, 929-961.
- 136 M. C. Biesinger, B. P. Payne, L. W. M. Lau, A. Gerson and R. S. C. Smart, Surf. Interface Anal., 2009, 41, 324-332.
- 137 N. M. Rodriguez, J. Mater. Res., 1993, 8, 3233-3250.
- 138 V. D. Blank, B. A. Kulnitskiy, I. A. Perezhogin, Y. L. Alshevskiy and N. V. Kazennov, Sci. Technol. Adv. Mater., 2009, 10, 015004.
- 139 F. Abild-Pedersen, J. K. Norskov, J. R. Rostrup-Nielsen, J. Sehested and S. Helveg, Phys. Rev. B: Condens. Matter Mater. Phys., 2006, 73, 115419.
- 140 S. Hofmann, G. Csanyi, A. C. Ferrari, M. C. Payne and J. Robertson, Phys. Rev. Lett., 2005, 95, 036101.
- 141 S. Saadi, F. Abild-Pedersen, S. Helveg, J. Sehested, B. Hinnemann, C. C. Appel and J. K. Norskov, J. Phys. Chem. C, 2010, 114, 11221-11227.
- 142 S. Helveg, C. Lopez-Cartes, J. Sehested, P. L. Hansen, B. S. Clausen, J. R. Rostrup-Nielsen, F. Abild-Pedersen and J. K. Norskov, Nature, 2004, 427, 426-429.
- 143 S. Esconjauregui, C. M. Whelan and K. Maex, Carbon, 2009, 47, 659-669.

- 144 C. M. Sung and M. F. Tai, *Int. J. Refract. Met. Hard Mater.*, 1997, **15**, 237–256.
- 145 S. Takenaka, Y. Shigeta, E. Tanabe and K. Otsuka, *J. Catal.*, 2003, **220**, 468–477.
- 146 A. Garscadden, B. N. Ganguly, P. D. Haaland and J. Williams, *Plasma Sources Sci. Technol.*, 1994, 3, 239–245.
- 147 C. Park and R. T. K. Baker, *J. Phys. Chem. B*, 1999, **103**, 2453–2459.
- 148 V. I. Merkulov, A. V. Melechko, M. A. Guillorn, D. H. Lowndes and M. L. Simpson, *Appl. Phys. Lett.*, 2001, 79, 2970–2972.
- 149 R. T. K. Baker, Carbon, 1989, 27, 315-323.
- 150 W. B. Downs and R. T. K. Baker, *Carbon*, 1991, **29**, 1173–1179.
- 151 S. Motojima, S. Asakura, T. Kasemura, S. Takeuchi and H. Iwanaga, *Carbon*, 1996, **34**, 289–296.
- 152 M. A. Ermakova, D. Y. Ermakov, G. G. Kuvshinov and L. M. Plyasova, *J. Catal.*, 1999, **187**, 77–84.
- 153 I. Martin-Gullon, J. Vera, J. A. Conesa, J. L. Gonzalez and C. Merino, *Carbon*, 2006, 44, 1572–1580.
- 154 R. T. K. Baker, M. S. Kim, A. Chambers, C. Park and N. M. Rodriguez, *Stud. Surf. Sci. Catal.*, 1997, **111**, 99–109.
- 155 R. T. K. Baker, J. J. Chludzinski and R. D. Sherwood, *Carbon*, 1985, 23, 245–254.
- 156 W. L. Yao, J. L. Wang, J. Yang and G. D. Du, *J. Power Sources*, 2008, **176**, 369–372.
- 157 S. Arai and M. Endo, *Electrochem. Commun.*, 2003, 5, 797–799.
- 158 H. Wu, R. Zhang, X. X. Liu, D. D. Lin and W. Pan, *Chem. Mater.*, 2007, **19**, 3506–3511.
- 159 R. Vieira, C. Pham-Huu, N. Keller and M. J. Ledoux, *Chem. Commun.*, 2002, 954–955, DOI: 10. 1039/b202032g.
- 160 E. S. Steigerwalt, G. A. Deluga, D. E. Cliffel and C. M. Lukehart, *J. Phys. Chem. B*, 2001, **105**, 8097–8101.
- 161 C. Singh, T. Quested, C. B. Boothroyd, P. Thomas, I. A. Kinloch, A. I. Abou-Kandil and A. H. Windle, *J. Phys. Chem. B*, 2002, **106**, 10915–10922.
- 162 F. Ding, P. Larsson, J. A. Larsson, R. Ahuja, H. M. Duan, A. Rosen and K. Bolton, *Nano Lett.*, 2008, **8**, 463–468.
- 163 N. M. Rodriguez, M. S. Kim and R. T. K. Baker, *J. Phys. Chem.*, 1994, **98**, 13108–13111.
- 164 Y. Yamada, Y. Hosono, N. Murakoshi, N. Higashi, H. Ichioka, T. Miyake, N. Ikenaga and T. Suzuki, *Diamond Relat. Mater.*, 2006, **15**, 1080–1084.
- 165 I. Willems, Z. Konya, J. F. Colomer, G. Van Tendeloo, N. Nagaraju, A. Fonseca and J. B. Nagy, *Chem. Phys. Lett.*, 2000, 317, 71–76.
- 166 F. G. Sun, J. T. Wang, D. H. Long, W. M. Qiao, L. C. Ling, C. X. Lv and R. Cai, J. Mater. Chem. A, 2013, 1, 13283–13289.
- 167 L. L. He, M. H. Fan, B. Dutcher, S. Cui, X. D. Shen, Y. Kong, A. G. Russell and P. McCurdy, *Chem. Eng. J.*, 2012, **189**, 13– 23.
- 168 C. L. Cheung, A. Kurtz, H. Park and C. M. Lieber, *J. Phys. Chem. B*, 2002, **106**, 2429–2433.
- 169 O. C. Carneiro, N. M. Rodriguez and R. T. K. Baker, *Carbon*, 2005, **43**, 2389–2396.

- 170 N. Krishnankutty, N. M. Rodriguez and R. T. K. Baker, *J. Catal.*, 1996, **158**, 217–227.
- 171 R. A. Vansanten and W. M. H. Sachtler, *Surf. Sci.*, 1977, **63**, 358–369.
- 172 M. L. Burke and R. J. Madix, *J. Am. Chem. Soc.*, 1991, **113**, 1475–1484.
- 173 P. S. Kumbhar, M. R. Kharkar, G. D. Yadav and R. A. Rajadhyaksha, *J. Chem. Soc., Chem. Commun.*, 1992, 7, 584–586.
- 174 A. Tanaka, S. H. Yoon and I. Mochida, *Carbon*, 2004, 42, 591–597.
- 175 N. M. Rodriguez, A. Chambers and R. T. K. Baker, *Langmuir*, 1995, **11**, 3862–3866.
- 176 H. Y. Wang and R. T. K. Baker, J. Phys. Chem. B, 2004, 108, 20273–20277.
- 177 M. S. Kim, N. M. Rodriguez and R. T. K. Baker, *J. Catal.*, 1992, **134**, 253–268.
- 178 Y. M. Li, W. Kim, Y. G. Zhang, M. Rolandi, D. W. Wang and H. J. Dai, *J. Phys. Chem. B*, 2001, **105**, 11424–11431.
- 179 X. X. Zhang, Z. Q. Li, G. H. Wen, K. K. Fung, J. L. Chen and Y. D. Li, *Chem. Phys. Lett.*, 2001, 333, 509–514.
- 180 S. B. Sinnott, R. Andrews, D. Qian, A. M. Rao, Z. Mao, E. C. Dickey and F. Derbyshire, *Chem. Phys. Lett.*, 1999, 315, 25–30.
- 181 C. L. Marotta, R. Terry and K. Baker, *J. Mol. Catal. A: Chem.*, 2003, **195**, 209–218.
- 182 R. Andrews, D. Jacques, D. L. Qian and T. Rantell, *Acc. Chem. Res.*, 2002, **35**, 1008–1017.
- 183 M. L. Toebes, J. H. Bitter, A. J. van Dillen and K. P. de Jong, *Catal. Today*, 2002, **76**, 33–42.
- 184 S. S. Tzeng, K. H. Hung and T. H. Ko, *Carbon*, 2006, **44**, 859–865.
- 185 R. T. K. Baker, M. S. Kim, A. Chambers, C. Park and N. M. Rodriguez, *Stud. Surf. Sci. Catal.*, 1997, **111**, 99–109.
- 186 S. Amelinckx, X. B. Zhang, D. Bernaerts, X. F. Zhang, V. Ivanov and J. B. Nagy, *Science*, 1994, **265**, 635–639.
- 187 N. Armenise, N. Tahiri, N. N. H. M. Eisink, M. Denis, M. Jager, J. G. De Vries, M. D. Witte and A. J. Minnaard, *Chem. Commun.*, 2016, **52**, 2189–2191.
- 188 T. S. Moraes, R. C. R. Neto, M. C. Ribeiro, L. V. Mattos, M. Kourtelesis, S. Ladas, X. Verykios and F. B. Noronha, *Appl. Catal., B*, 2016, **181**, 754–768.
- 189 P. García-Muñoz, G. Pliego, J. A. Zazo, A. Bahamonde and J. A. Casas, *J. Environ. Chem. Eng.*, 2016, 4, 542–548.
- 190 L. Xu, L. Guo, G. Hu, J. Chen, X. Hu, S. Wang, W. Dai and M. Fan, *RSC Adv.*, 2015, 5, 37964–37969.
- 191 L. B. Avdeeva, D. I. Kochubey and S. K. Shaikhutdinov, *Appl. Catal.*, *A*, 1999, 177, 43–51.
- 192 S. P. Chai, S. H. S. Zein and A. R. Mohamed, *Chem. Phys. Lett.*, 2006, **426**, 345–350.
- 193 L. B. Avdeeva, T. V. Reshetenko, Z. R. Ismagilov and V. A. Likholobov, *Appl. Catal.*, *A*, 2002, 228, 53–63.
- 194 L. Dussault, J. C. Dupin, C. Guimon, M. Monthioux, N. Latorre, T. Ubieto, E. Romeo, C. Royo and A. Monzon, J. Catal., 2007, 251, 223–232.
- 195 Y. Nishiyama and Y. Tamai, J. Catal., 1974, 33, 98-107.

- 196 A. Monzon, N. Latorre, T. Ubieto, C. Royo, E. Romeo, J. Villacampa, L. Dussault, J. C. Dupin, C. Guimon and M. Montioux, Catal. Today, 2006, 116, 264-270.
- 197 N. Bayat, M. Rezaei and F. Meshkani, Int. J. Hydrogen Energy, 2016, 41, 5494-5503.
- 198 H. Ogihara, S. Takenaka, I. Yamanaka, E. Tanabe, A. Genseki and K. Otsuka, J. Catal., 2006, 238, 353-360.
- 199 D. Wakeham, D. G. Crivoi, F. Medina, A. M. Segarra and M. W. Rutland, J. Colloid Interface Sci., 2016, 469, 263-268.
- 200 S. Schaubach, K. Gebauer, F. Ungeheuer, L. Hoffmeister, M. K. Ilg, C. Wirtz and A. Furstner, Chem.-Eur. J., 2016, 22, 8494-8507.
- 201 S. Takenaka, Y. Shigeta, E. Tanabe and K. Otsuka, J. Phys. Chem. B, 2004, 108, 7656-7664.
- 202 H. Ogihara, S. Takenaka, I. Yamanaka, E. Tanabe, A. Genseki and K. Otsuka, J. Catal., 2006, 238, 353-360.
- 203 R. L. Vander Wal, T. M. Ticich and V. E. Curtis, Carbon, 2001, 39, 2277-2289.
- 204 S. Takenaka, M. Ishida, M. Serizawa, E. Tanabe and K. Otsuka, J. Phys. Chem. B, 2004, 108, 11464-11472.

- 205 J. L. Chen, Y. D. Li, Z. Q. Li and X. X. Zhang, Appl. Catal., A, 2004, 269, 179-186.
- 206 T. de Los Arcos, M. G. Garnier, J. W. Seo, P. Oelhafen, V. Thommen and D. Mathys, J. Phys. Chem. B, 2004, 108,
- 207 H. Kanzow and A. Ding, Phys. Rev. B: Condens. Matter Mater. Phys., 1999, 60, 11180-11186.
- 208 J. Zhao, A. Martinez-Limia and P. B. Balbuena, Nanotechnology, 2005, 16, S575-S581.
- 209 Y. K. Y. Homma, T. Ogino, D. Takagi, R. Ito, Y. J. Jung and P. M. Ajayan, J. Phys. Chem. B, 2003, 107, 12161-12164.
- 210 C. T. W. C. Mattevi, S. Hofmann, R. Blume, M. Cantoro, C. Ducati, C. Cepek, A. Knop-Gericke, S. Milne, C. Castellarin-Cudia, S. Dolafi, A. Goldoni, R. Schloegl and J. Robertson, J. Phys. Chem. C, 2008, 112, 12207-12213.
- 211 P. Wang, F. Song, R. Amal, Y. H. Ng and X. L. Hu, ChemSusChem, 2016, 9, 472-477.
- 212 T. Y. Ma, J. Ran, S. Dai, M. Jaroniec and S. Z. Qiao, Angew. Chem., Int. Ed., 2016, 9, 472-477.